

Expulsion of abnormally pressured fluids along faults

Sheila J. Roberts¹ and Jeffrey A. Nunn

Department of Geology and Geophysics, Louisiana State University, Baton Rouge

Larry Cathles and Francois-Dominique Cipriani

Department of Geological Sciences, Cornell University, Ithaca, New York

Abstract. Numerical simulations of fluid flow and heat transport in the South Eugene Island minibasin, offshore Louisiana, show that expulsion of geopressured fluids along faults can produce temperature and pressure anomalies similar to those observed in the area. In the simulations, abnormally pressured fluid moves along the fault through a fracture network. A thermal anomaly forms adjacent to the fault, while a larger fluid pressure anomaly extends into sediments on either side. Results from constant fault permeability simulations indicate that (1) geopressured sediments must be relatively permeable ($5 \times 10^{-17} \text{ m}^2$) for expulsion to occur, (2) the size of thermal anomalies depend on the depth to which the fault is hydraulically open, and (3) fluid is vertically transported into shallow sediments when fault permeability is high, while lateral transport along deeper sands dominates when fault permeability is low. Excess fluid pressure in abnormally pressured sediments drops to half its original value throughout much of the minibasin after 10,000 years of expulsion; the associated thermal anomaly is also larger than observations, suggesting expulsion is not continuous. Variable fault permeability simulations, in which compaction of fault zone sediments closes the fracture network, indicate that fault permeability decreases by 1-2 orders of magnitude 1-200 years after expulsion begins. Thermal and baric anomalies from variable permeability simulations are smaller than from constant permeability simulations and are more consistent with available data. Faults must remain permeable for 20-30 years to produce thermal and baric anomalies similar to those observed in the area.

Introduction

Abnormally high fluid pressures are commonly observed in thick sequences of clay-rich sediments in many basins [e.g., *Bethke*, 1986; *Hunt*, 1990]) and along some convergent margins [e.g., *Westbrook and Smith*, 1983]. A variety of evidence suggests that fault zones in these and other settings may act as either low-permeability barriers that impede and compartmentalize fluid flow or as relatively permeable conduits along which flow is focused [*Smith*, 1980; *Hooper*, 1991; *Knipe*, 1993; *Haneberg*, 1995; *Lopez and Smith*, 1995]. A fault may change from a barrier to a conduit or vice versa by formation/collapse of fracture networks [*Brown*, 1995] or displacement of aquifers/aquitards across the fault zone [*Wieck et al.*, 1995] during active faulting.

¹Now at Department of Geology, Bowling Green State University, Bowling Green, Ohio.

Copyright 1996 by the American Geophysical Union.

Paper number 96JB02653.
0148-0227/96/96JB-02653\$09.00

Although the presence of oil and gas reservoirs trapped along faults clearly demonstrates that many faults are relatively impermeable, there is a variety of evidence supporting the existence of some episodically permeable fault zones in overpressured, clay-rich sediments. This evidence includes temperature, pressure, and salinity anomalies recorded in wells [e.g., *Bennett and Hanor*, 1987; *Anderson*, 1993], mud volcanoes [e.g., *Hedberg*, 1974; *Henry et al.*, 1990], biotic communities [e.g., *Lewis and Cochrane*, 1990] and active venting sites [e.g., *J.C. Moore et al.*, 1990; *Aharon et al.*, 1992] observed on the sea floor, and seismic velocity anomalies [e.g., *G.F. Moore et al.*, 1990]. In these settings, periods of enhanced permeability along a fault may be associated with the formation of fractures in the fault zone [*Roberts and Nunn*, 1995; *Bekins et al.*, 1995] or movement along the fault [*Sibson*, 1990]. Expulsion of pore fluid along a fault can reduce fault zone permeability as the fracture network collapses due to the drop in fluid pressure, thermal expansion of wall rock adjacent to fractures, and/or precipitation of mineral cements along the fault zone [e.g., *Lowell*, 1990; *Knipe*, 1993; *Brown*, 1995; *Roberts and Nunn*, 1995].

The episodic release of fluid along fault zones has the potential to transfer large amounts of matter and energy into the adjacent sediments [Lopez and Smith, 1995; Roberts and Nunn, 1995] and may influence migration and localization of hydrocarbon-bearing and ore-forming fluids. The amount of fluid transported along a fault and the consequences of expulsion depend on both the frequency and duration of events. Cathles and Smith [1983], who first proposed that abnormally pressured fluids in sedimentary basins are episodically expelled into overlying strata, predicted that events shorter than 1000 years occurring every 1 Myr could explain mineral zonation patterns and temperatures recorded in Mississippi Valley Type ore deposits. Alternatively, Hunt [1990] suggested that cycles of pressurization, fracturing, and expulsion in abnormally pressured sediments occur on a time span of several thousand years.

Numerical models simulating heat and mass transport along fault zones provide additional constraints on the duration and consequences of expulsive events. For example, Ranganathan and Hanor [1989] and Ranganathan [1992] tested the hypothesis that expulsion of geopressured fluids along the flanks of the Welsh salt dome in southwestern Louisiana formed a perched brine plume. Their results show that brine plumes form quickly (<10,000 years) and must be young or formed by a continuous venting process in order to be observed today. In a more recent study, Williams and Ranganathan [1994] showed that thermal plumes around salt domes can form in less than 3000 years. Cipriani *et al.* [1993] reproduced temperature anomalies observed in the South Eugene Island area, offshore Louisiana, by expelling all excess fluids along a growth fault in only 30 years. Although these models indicate that expulsion events are short lived, it is impossible to predict how long a given event will last because expulsion is viewed as a kinematic process in which the permeability of the fault remains constant throughout the venting process.

Roberts and Nunn [1995] used a dynamic one-dimensional numerical model to quantitatively evaluate the consequences of episodic fluid expulsion and to estimate the frequency and duration of events. They assumed fractures formed across a low-permeability layer when fluid pressure exceeded the minimum confining stress of adjacent sediments, initiating an expulsion event. As fluid is withdrawn and the surrounding sediments compact, the width and permeability of the fracture decrease. Results of their model demonstrate that the amount of fluid transported upward is dependent on the permeability of sediments above and below the top of geopressure and the amount of time required to close any open flow paths in the fault zone. Furthermore, they predict that a single fracture emplaced in clay-rich sediments will close 20-50 years after expulsion begins and that temperature anomalies of the order of tens of degrees Celsius can form in the sediments directly

above the top of geopressure in less than 100 years. Finally, Roberts and Nunn [1995] show that in the absence of pressure generating processes such as sedimentation or hydrocarbon generation, 10,000-500,000 years are required to replace the expelled fluid from deeper in the geopressured zone and to build fluid pressure back to the levels required to initiate another event. This estimate is probably an upper bound as fluid should also flow laterally toward the fault from surrounding sediments.

Although Roberts and Nunn [1995] demonstrated that episodic expulsion of abnormally pressured fluids along a vertical fault can form significant thermal anomalies in a relatively short period of time, they were unable to assess the importance of the lateral movement of fluid both toward and away from the fault zone. A simple 1-D model also cannot predict fluid migration in a hydrostratigraphically complex minibasin containing multiple thin sand/shale layers offset across a fault zone. Furthermore, their results give no indication as to the horizontal extent of the thermal and baric anomalies that form and expand laterally away from the fault zone as expulsion continues. These issues are addressed in the present investigation, in which a two-dimensional finite element model is used to assess the role of faults as conduits for fluid flow in clay-rich, partially consolidated sedimentary sequences by numerically simulating fluid expulsion and heat transport in the South Eugene Island area, offshore Louisiana. In the model, faults become permeable when elevated fluid pressure opens an interconnected network of microfractures in the fault zone. Two types of simulations are investigated: those in which fault permeability remains constant and those in which fault permeability decreases as fluid is expelled. Results from these simulations constrain the quantity of fluid expelled from the geopressured sediments and illustrate how this fluid moves upward through the overlying, hydrostatically pressured strata. Temperature and pressure fields predicted from the simulations are also compared to field data to determine which of the simulations (constant or variable fault permeability) best explain thermal and baric anomalies observed in the South Eugene Island area.

Fluid Flow and Abnormally Pressured Sediments

A number of processes may contribute to the development of abnormally high fluid pressures in sediments [Neuzil, 1995]. In general, overpressured sediments are both undercompacted relative to similar hydrostatically pressured sediments at the same depth and clay rich, suggesting that rapid loading and disequilibrium compaction are important pressure-generating mechanisms [e.g., Dickinson, 1953; Bredehoeft and Hanshaw, 1968; Bethke, 1985; Harrison and Summa, 1991]. Numerical simulations [Bethke, 1986; Harrison and Summa, 1991] indicate that regional patterns of overpressure,

like those observed in the Gulf of Mexico, can form from disequilibrium compaction alone when vertical shale permeabilities are of the order of 10^{-17} to 10^{-21} m² on a basin-wide scale. However, careful analysis of porosity and fluid pressure as a function of depth in the South Eugene Island area, offshore Louisiana, suggests that only 75% of the observed overpressures formed in response to compaction disequilibrium [Hart *et al.*, 1995]. The change in fluid volume accompanying the transformation of solid kerogen into liquid and gaseous hydrocarbons is another potentially important pressure-generating mechanism [e.g., Hedberg, 1974; Spencer, 1987; Bredehoeft *et al.*, 1994; Yassir and Bell, 1994] and may explain the existence of abnormally high fluid pressures that cannot be attributed to compaction disequilibrium, such as the South Eugene Island area [Hart *et al.*, 1995] and those basins where there is currently no rapid influx of sediment (e.g., the Anadarko Basin [Deming, 1994]). Other processes that may contribute to the formation of overpressures include deformation along convergent margins [Shi *et al.*, 1989; Sreaton *et al.*, 1990], the release of fluid from dehydration reactions [e.g., Powers, 1967; Bethke, 1986], and aquathermal pressuring [e.g., Barker, 1972; Sharp, 1983].

Some workers have argued that generation and maintenance of abnormally high fluid pressures require the presence of a low-permeability barrier, which they call a seal, along the upper boundary of the overpressured region [Hunt, 1990; Powley, 1990]. As evidence, they cite reports indicating that the top of overpressure may cut across lithologic boundaries in some areas. Several theories regarding the nature of these barriers have been proposed; these include diagenetic seals, such as chemical cements [Hunt, 1990] or the smectite to illite transformation [Bruce, 1984; Freed and Peacor, 1989], seals formed by the collapse of secondary porosity [Weedman *et al.*, 1992], shale membrane seals [Fowler, 1970], and capillary seals formed when an exsolved gas phase is present in the pores [Downey, 1984; Antonellini and Aydin, 1994]. Ortoleva *et al.* [1995] suggest that compartment bounding barriers may form spontaneously via feedback between chemical, transport and mechanical processes as a basin evolves.

The potential for fracture development and permeability enhancement in abnormally pressured sediments provides further supporting evidence that some kind of low-permeability barrier may be needed to locally maintain abnormal fluid pressures, especially in areas where fluid pressures approach lithostatic values. Palciauskas and Domenico [1980] showed that it is theoretically possible for fractures to develop in overpressured strata undergoing burial. Crosscutting relationships and alteration halos along fracture margins in geopressured shales of the Texas Gulf Coast observed by Capuano [1993] document the existence of open fractures, which dramatically increase permeability, in some geopressured shales. Experiments conducted by Jouniaux *et al.* [1994] support the conclusion that the perme-

ability of some clay-rich sediments increases with stress. They measured the permeability of a claystone from the Nankai prism under stress and showed that the permeability of such sediments is low prior to failure and much higher and strongly dependent on fluid pressure after failure. Similar experiments by Brown [1995] showed that the permeability of fault zone sediments from the Cascadia accretionary wedge varied by 3 orders of magnitude as pore fluid pressure changed.

Formation of a fracture network through the boundary separating overpressured and hydro pressured sediments will result in expulsion of the abnormally pressured fluid into the adjacent sediments. Although it has been argued that expulsion is widespread and diffuse in some areas [Davis *et al.*, 1990], there is compelling evidence that expulsion of fluid from some abnormally pressured sediments is focused along fault zones. Measured flow rates and mass balance calculations indicate that fluid flow focused along faults in convergent margin settings is not steady state, but rather that individual vent sites are relatively short-lived features [Carson *et al.*, 1990; Fisher and Hounslow, 1990; Foucher *et al.*, 1990]. A similar conclusion was reached by Roberts and Nunn, 1995], who suggested expulsion from geopressured sediments in basins like the Gulf of Mexico is episodic, with individual events lasting less than 100 years.

Observations suggesting that fluid flow along fault zones is transient and episodic imply that some mechanism actively reduces fault zone permeability as fluid is expelled. A number of processes have the potential to reduce permeability, including precipitation of mineral phases along flow paths and thermal expansion or compaction of sediments adjacent to the fracture network. Chemical healing, or the dissolution of minerals in high energy environments adjacent to a fracture and precipitation in lower-energy environments within the fracture, efficiently closes microfractures but leaves larger fractures through which fluid flows open [Hickman and Evans, 1987; Brantley *et al.*, 1990]. Thermodynamic arguments suggest quartz and calcite can be deposited along a flow path when pressure decreases [Bruton and Helgeson, 1983; Capuano, 1990]. However, we are unaware of any areas in which these minerals have been identified as fracture filling in overpressured basin sediments, suggesting precipitation of mineral phases along fracture walls is not an important permeability reducing mechanism for the study discussed herein.

High-pressure experiments [Jouniaux *et al.*, 1994; Brown, 1995] and pressure drawdown tests [Anderson *et al.*, 1994] demonstrate that the permeability of incompletely consolidated, clay-rich sediments is a strong function of effective stress and that permeability decreases dramatically as fluid pressure drops. These data suggest that as fluid pressure drops in the geopressured section in response to expulsion, compaction of sediments in and around the fault zone is an important permeability reducing mechanism. Lowell [1990]

showed that thermal expansion of wall rocks may also reduce the width and permeability of fracture networks. His results indicate that 100- μm fractures spaced 1 m apart can be closed by a 10°C increase in temperature. However, our results (discussed below) show that the maximum thermal anomaly forms not at the boundary separating geopressured and hydrostatically pressured sediments but in sediments 200-500 m above the boundary. For this reason, thermoelastic sealing of fractures should become more important in the upper reaches of the fault zone than at the boundary separating hydrostatically pressured sediments from the underlying geopressured section. We therefore assume that the primary permeability-reducing mechanism in the fault zone is compaction of sediments adjacent to the fault zone.

South Eugene Island

The South Eugene Island Block 330 area minibasin, located in the Gulf of Mexico, offshore Louisiana (Figure 1), contains one of the world's largest Pleistocene oil and gas fields [Holland *et al.*, 1990; Anderson, 1993]. The basin formed in response to rapid Plio-Pleistocene sedimentation and concomitant withdrawal of an allochthonous salt sheet [Holland *et al.*, 1990; Alexander and Flemings, 1995]. Sediment deposition in the minibasin has been divided into three regimes by Alexander and Flemings [1995]: a prodelta regime, during which deep deltaic and turbiditic sediments overlain by a thick transgressive shale were deposited, a stalled-shelf regime, during which progradational shelf-edge delta sediments were deposited, and a bypass regime, during which coastal plain sediments were deposited. Each de-

positional environment corresponds to a distinct fluid pressure regime [Hart *et al.*, 1995]; the coastal plain sediments are hydrostatically pressured, the progradational deposits lie in a pressure transition regime, and the underlying turbidites are geopressured. Careful analysis of porosity and fluid pressure as a function of depth in the area suggests that only 75% of the observed overpressures formed in response to compaction disequilibrium; other processes are responsible for the remaining 25% of the overpressure [Hart *et al.*, 1995].

A number of independent observations suggest that hydrocarbon-bearing fluids have recently been expelled from geopressured sediments into overlying oil and gas reservoirs along a growth fault in the South Eugene Island area [Anderson *et al.*, 1994]. Fluid pressure is elevated over a broad (~5 km) region around the fault zone (Figure 2a), while a large thermal anomaly (~10-20°C) is restricted to the sediments immediately adjacent to the fault (Figure 2b) [Anderson *et al.*, 1991]. Additional evidence supporting recent or active fluid flow in the area includes unusually slow reservoir depletion, significant differences in reflection strength seen on three-dimensional seismic surveys conducted in 1985 and 1988, and changes in oil and gas chemistry [Anderson *et al.*, 1991; Anderson, 1993]. Furthermore, geochemical data suggest that both brines [Losh and Wood, 1994] and hydrocarbons [Whelan *et al.*, 1994a] in the South Eugene Island area reservoirs originated from Cretaceous or older rocks, implying significant vertical transport of fluid. Based on these data, Anderson *et al.* [1994] and Whelan *et al.* [1994b] suggest that hydrocarbons expelled from deeper source rocks migrated into the overpressured turbidite sand layers, where they were stored in temporary reservoirs. A recent migration event moved the hydrocarbons from the overpressured sediments to their present location.

To further test the hypothesis that fluid is actively migrating along the growth fault, the Global Basins Research Network (GBRN) took over a Pennzoil-operated development well, called the Pathfinder well, in the South Eugene Island area and extended it through the fault zone [Anderson *et al.*, 1994]. Whole coring, extensive logging, and stress and production testing were conducted in the well to determine in situ conditions within and surrounding the fault zone. Drill stems tests in a perforated and fracture-packed interval of the fault zone indicate that the permeability of the geopressured sediments is strongly dependent on fluid pressure [Anderson *et al.*, 1994]. At a drawdown pressure of 0.55 MPa, the measured permeability of fault zone sediments was greater than 10^{-13} m². However, sediment permeability had decreased to less than 10^{-16} m² at drawdown pressures of more than 20.7 MPa. The decrease in permeability with decreasing pore fluid pressure is interpreted as the result of collapse of the fracture network around the well [Anderson *et al.*, 1994; Roberts and Nunn, 1995].

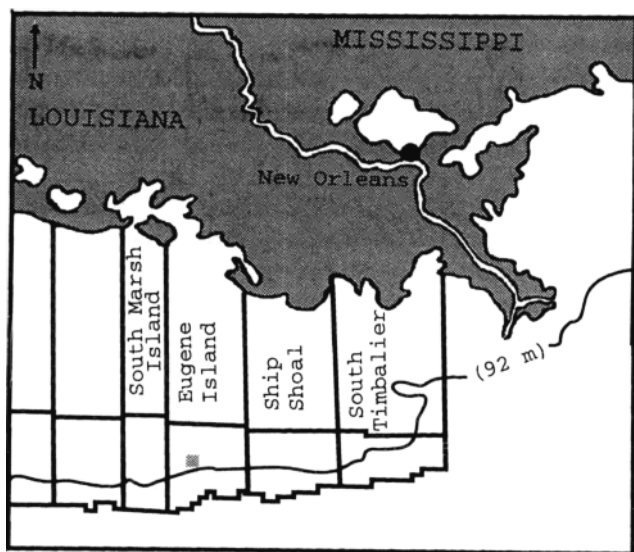


Figure 1. Location map of the South Eugene Island area. The shaded square just north of the 92 m water depth contour shows the location of the study area (modified from L. L. Alexander and P. B. Flemings, [1995], reprinted by permission of the American Association of Petroleum Geologists).

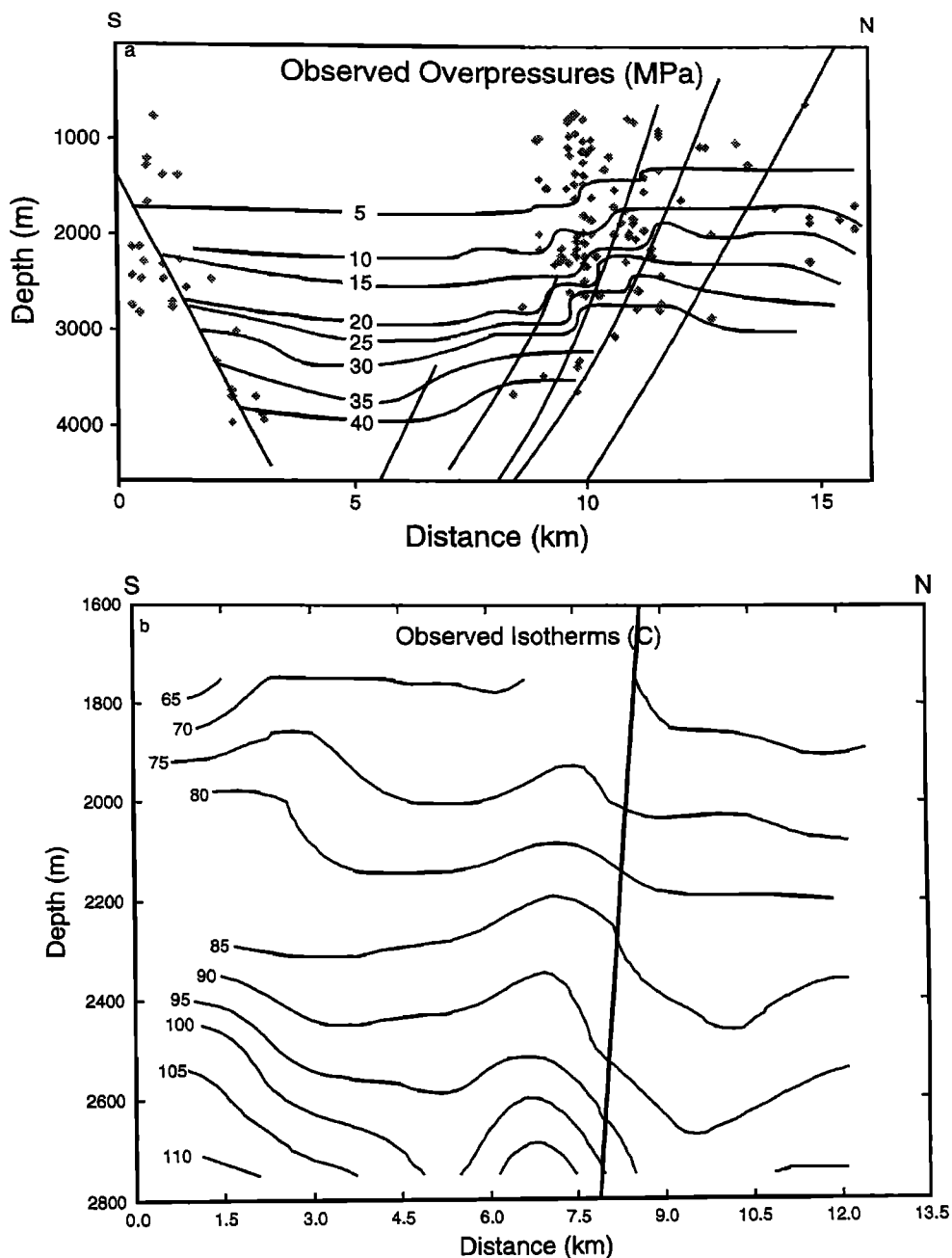


Figure 2. (a) Excess fluid pressure (modified from *Flemings et al.*, [1994]) and (b) temperature (data obtained from G. Guerin (unpublished data, 1996)) in the South Eugene Island minibasin. The shaded diamonds in Figure 2a represent the location of wells projected onto a 2-D plane. The top of geopressure is located at a depth of 2000 m. Note that the scale is not the same for Figures 2a and 2b.

The Model

Mathematical Representation of Fluid Expulsion

The purpose of the present communication is to simulate the effects of fluid expulsion and associated heat transport within part of a geopressed minibasin on timescales of hundreds to thousands of years. Therefore we do not account for any pressure generating mecha-

nisms (e.g., disequilibrium compaction related to sedimentation) or internal fluid sources (e.g., clay dehydration, hydrocarbon maturation), which become important only over much longer time spans [e.g., *Harrison and Summa*, 1991]. The initial fluid pressure within the basin is instead specified as an initial condition. Furthermore, we assume that deformation of the matrix associated with fluid expulsion is small (allowing us to use a fixed reference frame), individual mineral grains

and the fluid are incompressible, and thermal expansion of the solid grains and the porous body are neglected. Under these circumstances, conservation of fluid mass can be expressed as

$$\beta \frac{\partial P}{\partial t} - \alpha_f \phi \frac{\partial T}{\partial t} + \frac{1}{\rho_f} \nabla \cdot (\rho_f \mathbf{q}) = 0 \quad (1)$$

where β is the bulk compressibility of the porous body, P is the fluid pressure, α_f is the coefficient of thermal expansion for the fluid phase, ϕ is the porosity, T is the temperature, ρ_f is the fluid density, and \mathbf{q} is the volume flux of fluid. The first term in (1) reflects changes in pore volume associated with changes in fluid pressure, the second term represents changes in the density of pore fluids associated with changes in temperature, and the last term gives the rate of fluid outflow. Equation (1) is simplified from *Palciauskas and Domenico* [1989].

It is convenient to subtract the cold water hydrostatic gradient from the pressure term, $P = P_{\text{ex}} + \rho_o g z$ where P_{ex} is the excess fluid pressure, g is gravitational acceleration, and ρ_o is the reference cold water density. Note that excess fluid pressure is related to the more familiar equivalent freshwater head, h , by $P_{\text{ex}} = \rho_o g h$. Equation (1) then becomes

$$\beta \frac{\partial P_{\text{ex}}}{\partial t} - \alpha_f \phi \frac{\partial T}{\partial t} + \frac{1}{\rho_f} \nabla \cdot (\rho_f \mathbf{q}) = 0 \quad (2)$$

According to Darcy's law, the volume flux of fluid is given by

$$\mathbf{q} = -\frac{k}{\mu} [\nabla (P + \rho_f g z)] \quad (3)$$

or again subtracting the cold water hydrostatic gradient,

$$\mathbf{q} = -\frac{k}{\mu} [\nabla (P_{\text{ex}} + \rho_{\text{ex}} g z)] \quad (4)$$

where k is the intrinsic permeability of the medium, μ is the kinematic viscosity of the fluid, and $\rho_{\text{ex}} = \rho_f - \rho_o$. The first term in equation (4) represents fluid flow driven by spatial variations in fluid pressure and the second term represents convective fluid flow caused by fluid buoyancy.

Equation (2) is solved by separating the pressure-driven and buoyancy-driven parts of the flow field. In other words, we solve for fluid flow generated by excess fluid pressure assuming that fluid density is constant, and then we solve for buoyancy-driven fluid flow assuming hydrostatic fluid pressure. The total volume flux of fluid is obtained by combining the pressure-driven and the buoyancy-driven components of the flow field. This approach was used because it is numerically very stable.

Substituting (4) into (2) and setting $\rho_{\text{ex}} = 0$ gives the excess fluid pressure diffusion equation

$$\beta \frac{\partial P_{\text{ex}}}{\partial t} - \alpha_f \phi \frac{\partial T}{\partial t} + \frac{1}{\rho_f} \nabla \cdot \left(\frac{k \rho_f}{\mu} \nabla P_{\text{ex}} \right) = 0 \quad (5)$$

which is solved numerically for P_{ex} to give the pressure-

driven flow field. Setting $P_{\text{ex}} = 0$, assuming that the temperature term has been computed in (5), and using the Boussinesq approximation, (2) reduces to [Nunn, 1994]

$$\nabla \cdot \mathbf{q} = 0. \quad (6)$$

For a hydrostatically pressured system, substituting Eqn. 4 into Eqn. 6 gives the vorticity equation (Nunn, 1994)

$$\frac{\partial}{\partial x} \left(\frac{\mu}{k_x} \frac{\partial \psi}{\partial x} \right) + \frac{\partial}{\partial z} \left(\frac{\mu}{k_z} \frac{\partial \psi}{\partial z} \right) = -g \frac{\partial \rho_{\text{ex}}}{\partial x} \quad (7)$$

where ψ is the stream function. The buoyancy-driven fluid flow is derived from the spatial derivatives of the streamfunction solution to (7). The total volume fluid flux is obtained from

$$\mathbf{q} = -\frac{k}{\mu} \nabla P_{\text{ex}} + \nabla \times \psi \quad (8)$$

For the simulations presented herein, buoyancy-driven fluid flow associated with spatial variations in temperature is small compared to the pressure-driven flow.

Heat transport by conduction and advection in a fixed reference frame is described by

$$\rho_b C_b \frac{\partial T}{\partial t} - \nabla \cdot (K_b \nabla T) + \mathbf{q} \cdot \nabla \rho_f C_f T = 0 \quad (9)$$

where ρ , C , and K are the density, heat capacity, and thermal conductivity, respectively, and T is the temperature. The subscript b refers to bulk (matrix and fluid) properties and the subscript f refers to fluid properties. Equation (9) is derived through an assumption of conservation of energy and Fourier's law of heat conduction [Smith and Chapman, 1983].

Equations (5), (7), (8) and (9) were converted into finite element form using the Galerkin method on quadrilateral elements with linear basis functions [Baker and Pepper, 1991]; transient solutions to the resulting equations are obtained using the 2-D finite element Access-BasinTM software package. In the present study, the solution to each equation is iteratively computed using a fully implicit, Newton-Raphson technique. Fluid density is updated after each iteration of (9).

Fault Permeability

In the variable fault permeability simulations, fault permeability is dynamically computed at each time step as a function of the fluid pressure in the fault zone just below the low permeability layer. Following *Roberts and Nunn* [(1995), the fault zone is represented by n parallel fractures per horizontal meter along the fault. Each fracture has a width of w and instantaneously opens when fluid pressure exceeds the strength of surrounding rocks, approximately 85% of the lithostatic stress in the Gulf of Mexico [Engelder, 1993]. Fault zone permeability, k_f , is calculated using the parallel plate model [Snow, 1968]

$$k_f = \frac{nw^3}{12} \quad (10)$$

As fluid pressure drops and sediments in the fault zone compact, the width of fractures decrease. Although compaction is a plastic response to increasing stress, we assume that materials in the fault zone respond elastically for the small change in stress (<5 MPa) required to close the fracture. This simplification allows us to represent the relationship between fluid pressure and fracture width with a linear equation

$$\frac{w - w_o}{l} = -m(P_c - P) \quad (11)$$

where w_o is the initial fracture width, l is a unit length (1 m), P is the current fluid pressure, P_c is the pressure at which the fracture opened, and m is a constant describing the compressibility of materials in the fault zone. We assume that permeability calculated at any given time does not vary along the length of the fault. This approximation is necessary because of computational limitations imposed by dynamically computing fault zone permeability as a function of fluid pressure. Even using this simple model, extremely small time

steps ($\ll 1$ year) must be used during the early stages of fluid venting to compute changes in fault zone permeability.

Stratigraphic Model

Stratigraphic data obtained from seismic lines [Alexander and Flemings, 1995] were used to construct a realistic north-south cross section through the South Eugene Island minibasin [Coehlo *et al.*, 1994] (Figure 3). The cross section was discretized into a finite element mesh containing quadrilateral elements which varied in size from 0.01 km in height by 0.02 km in width near the fault zone to 0.4 km in height and 1 km in width near the model boundaries. A thin (~25 m) low-permeability layer was placed at the top of geopressure in our model. Sediments beneath this layer are uniformly overpressured by 22 MPa and, with the exception of a single thin sand layer immediately below the low-permeability layer, are shale rich. The overlying hydro-pressured zone contains 11 sand layers, denoted as CA, DA, EA, GA, HB, JD, K, LF, MG, OI, and Lentic from top to bottom, separated by shale. The fault zone cuts through all but the uppermost three sands.

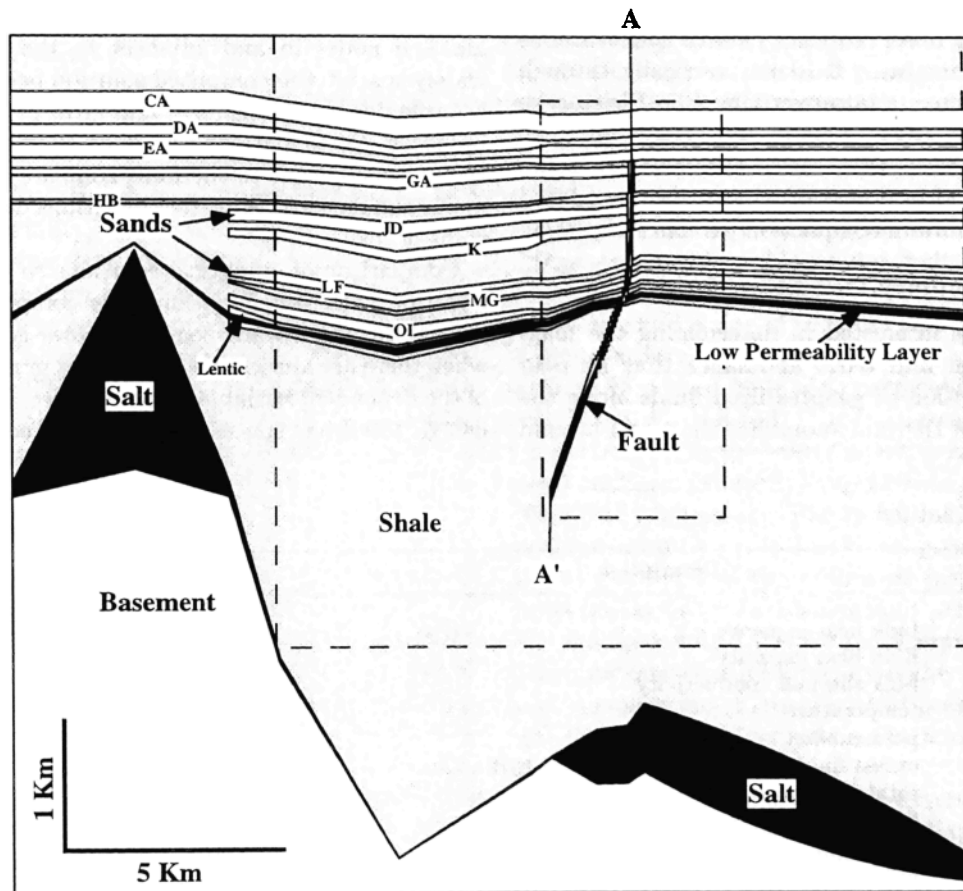


Figure 3. Two-dimensional N-S cross section through the South Eugene Island minibasin [Coehlo *et al.*, 1994] used in the simulations. The small box outlined by the dashed lines represents the area shown in Figures 4, 6, 10, and 12. The larger box outlined by the dashed lines represents the area shown by Figure 8. The line labeled A-A' shows location of the temperature profiles shown in Figures 5, 7, 11 and 13. Vertical exaggeration is 3:1.

Excess fluid pressure contours shown in Figure 2b [Flemings *et al.*, 1994] suggest that the transition zone separating hydrostatic from near lithostatic fluid pressures in the Eugene Island minibasin is thicker (several hundred meters) than the low-permeability layer (25 m) at the top of geopressure in our model. Alternatively, based on measurements in the Pathfinder well, Hart *et al.* [1995] infer that the transition zone is 100 m thick. However, data from the Pathfinder well are sparse, with essentially hydrostatic fluid pressures at the top of the fault zone (1250-2000 m depth) and near lithostatic values at the bottom (2100-2200 m depth). There are no data between 2000 and 2100 m depth, where the transition from hydrostatic to near lithostatic fluid pressures is located. Moreover, there is a sharp downward increase in shale porosity (and presumably permeability) from 20% to 30% at the base of the fault zone in the Pathfinder well. Hart *et al.* [1995] note that the lower values of porosity are from sidewall cores and may not be reliable. Given the uncertainties in available fluid pressure data, our present model is sufficient to quantitatively examine temperature and pressure anomalies generated in the hydro-pressured zone caused by episodic fluid expulsion. A low-permeability layer at the top of geopressure which is periodically breached along a fault zone is consistent with the following observations: (1) both hydrocarbons and brines have migrated 5-10 km vertically through geopressed sediments into overlying Plio-Pleistocene reservoirs [Whelan *et al.*, 1994b]; and (2) present pore fluid pressures in the geopressed zone are near lithostatic ($\sim 93\%$) and in excess of what can be produced solely by disequilibrium compaction [Hart *et al.*, 1995].

Initial and Boundary Conditions

Because we are interested in determining the magnitude of thermal and baric anomalies that form in response to expulsion of geopressed fluids along the fault zone and not thermal anomalies that form around

the salt domes, we assume that all sediments, including salt, have the same thermal conductivity, which is independent of porosity and temperature. As a result, temperature initially increases linearly with depth ($25^\circ\text{C}/\text{km}$), and all temperature perturbations predicted from our simulations can be attributed directly to fluid expulsion. We further assume pre-Tertiary sediments beneath the salt form an impermeable basement extending to a depth of 10 km. Temperature (20°C) and pressure (0 MPa) are kept constant at the top surface while constant gradients normal to the surface are maintained along the base and sides. Dirichlet boundary conditions are used for the stream function. Because expulsion is a local event which influences only those sediments within a few kilometers of the venting site, there is very little interaction with the boundaries in most of our simulations. Material properties used in the simulations are shown in Table 1 and Table 2.

Numerical Stability and Accuracy

The presence of a large pressure gradient at the top of geopressure, high-permeability contrasts between adjacent sand, shale, and fault zone elements, and high fault permeability cause pressure perturbations to form in the low-permeability elements (shales) adjacent to the fault zone immediately after fluid expulsion begins. If nodes in and adjacent to the fault zone are widely spaced, the computed solution becomes unstable as large perturbations form and grow as the simulation proceeds. Perturbations are much smaller and decay if the nodes adjacent to the fault zone are closely spaced; in our simulations, these perturbations decay in 10 time steps or less.

Comparison of analytical solutions to a 1-D diffusion equation with transient solutions computed using the Akcess.Basin software package shows good agreement when there are abrupt discontinuities in the initial value of the dependent variable. Furthermore, G. Lin (unpublished, 1996) has successfully reproduced the results of

Table 1. Nomenclature

Symbol	Description	Units	Value
C_b	bulk heat capacity	J/kg $^\circ\text{C}$	computed
C_f	fluid heat capacity	J/kg $^\circ\text{C}$	computed
K	bulk thermal conductivity	W/mK	2.5
T	temperature	$^\circ\text{C}$	computed
k	permeability	m^2	variable
P_{ex}	excess fluid pressure (pressure over hydrostatic)	MPa	computed
q	total fluid mass flux	$\text{kg}/\text{m}^2 \text{ s}$	computed
α	fluid thermal expansivity	$^\circ\text{C}^{-1}$	10^{-3}
β	long-term compressibility	MPa^{-1}	$\sim 4 \times 10^{-3}$
μ	kinematic viscosity	$\text{kg}/\text{m s}$	2×10^{-8}
ρ_b	bulk density	kg/m^3	computed
ρ_o	reference fluid density	kg/m^3	1000
ψ	stream function	m^2/s	computed

Table 2. Permeability Values Used in Simulations

Unit	Permeability
All simulations	
Sand permeability	
Horizontal	10^{-15} m^2
Vertical	10^{-16} m^2
Shale permeability	
horizontal	10^{-17} - 10^{-16} m^2
vertical	10^{-18} - 10^{-17} m^2
Permeability at top of geopressure	10^{-24} - 10^{-21} m^2
Constant permeability simulations	
Fault permeability	10^{-15} - $5 \times 10^{-14} \text{ m}^2$
Variable permeability simulations	
Compressibility	10^{-10} - 10^{-12} Pa^{-1}
Initial fracture width	10-100 μm
Number of fractures	1-5

Garven *et al.* [1993] and Smith and Chapman [1983] using the Akcess.basin software. Results of these tests demonstrate that the computational procedures used in the Akcess.basin software package are capable of predicting transient solutions to time dependent equations when there are abrupt changes in material properties.

Sensitivity Analysis

In the results presented below, we have attempted to simulate the hydrostratigraphy of the Eugene Island area as accurately as possible with available data and a tractable grid size. However, certain parameters, such as shale permeability, depth to which the seismically mapped fault zone is hydrologically open, and compaction coefficients for fault zone sediments, are poorly constrained. Thus we have conducted multiple simulations to show how our results depend on our choice of parameters. The sensitivity analysis also provides insight into the physical processes involved in fluid expulsion and heat transport.

Results

When the fracture network opens within the fault zone, overpressured fluid is free to move upward into the overlying sediments. Two models, constant and variable fault permeability, were analyzed to assess the consequences of such an event. In the constant fault permeability model, fault zone permeability remains constant as fluid flows from the geopressed sediments into the overlying section. In the variable fault permeability model, the permeability of the fault zone, calculated using equations (10) and (11), decreases as fluid pressure drops and sediment compaction closes open fractures.

Constant Fault Permeability Simulations

Excess fluid pressure and temperature predicted from the constant fault permeability model with $k_f = 10^{-14}$

m^2 at 25, 100, and 250 years after expulsion begins are shown in Figure 4. When an expulsion event begins, pore fluid from geopressed sediments adjacent to the fault moves rapidly along the fault zone and into the overlying sediments. Fluid flows preferentially into the sand layers intersected by the fault zone, as indicated by both higher fluid pressures in the sands relative to the interbedded shales and larger fluid velocities. Darcy fluid velocities in the sand layers are several hundred centimeters per year, while maximum velocities in the fault zone can exceed 10,000 cm/yr.

The pressure anomaly that forms in the overlying sediments after expulsion begins moves both outward and upward with time (Figure 4a-4c). This implies that the lower sand layers (LF, MG, OI, and Lentic) fill with expelled fluid sooner than stratigraphically higher sands (HB, JD, and K). The constant fault permeability model also predicts that some fluid from the geopressed sediments will begin to flow into the stratigraphically highest sand layers (CA, DA, EA, and GA) above the fault ~ 100 years after an expulsion event begins (Figure 4b).

Like the pressure anomaly, the thermal anomaly grows upward and outward with time, albeit at a much slower rate (Figures 4d-4f and Figure 5). The maximum thermal anomaly increases from 14°C 25 years after expulsion begins to over 30°C 250 years into an expulsion event. Although the thermal perturbation grows as expulsion continues, it is essentially confined to those sediments immediately adjacent to the fault zone. After 250 years of expulsion, isotherms in the upper 0.75 km of sediment (above the CA sand) are undisturbed, and the thermal anomaly extends less than 0.5 km into the sediments on either side of the fault zone (Figures 5 and 4f).

The size and shape of pressure and temperature anomalies that form in response to expulsion are dependent on both shale and fault zone permeability. When fault permeability is low (10^{-15} m^2), pressure and temperature anomalies in the overlying sediments are relatively small and form primarily in those sand layers just above the top of geopressure (Figure 6a and Figure 7a). The pressure drop observed in the geopressed sediments is also restricted to the sediments just below the low-permeability layer. Increasing fault permeability allows the expelled fluid to move more rapidly up the fault zone and into stratigraphically higher sands. As a result, temperature (Figure 7a) and pressure (Figures 4b and 6b) anomalies increase in size and move into shallower sediments.

The pressure anomaly is also extremely sensitive to shale permeability. As the permeability of shales in the simulations decreases, flow of geopressed fluid toward the fault zone is severely restricted (Figure 6c). When shale permeability is decreased by 1 order of magnitude, fluid pressure in the geopressed sediments drops only within 0.5 km of the fault. After 100 years of expulsion, fluid pressure remains virtually constant in the geopres-

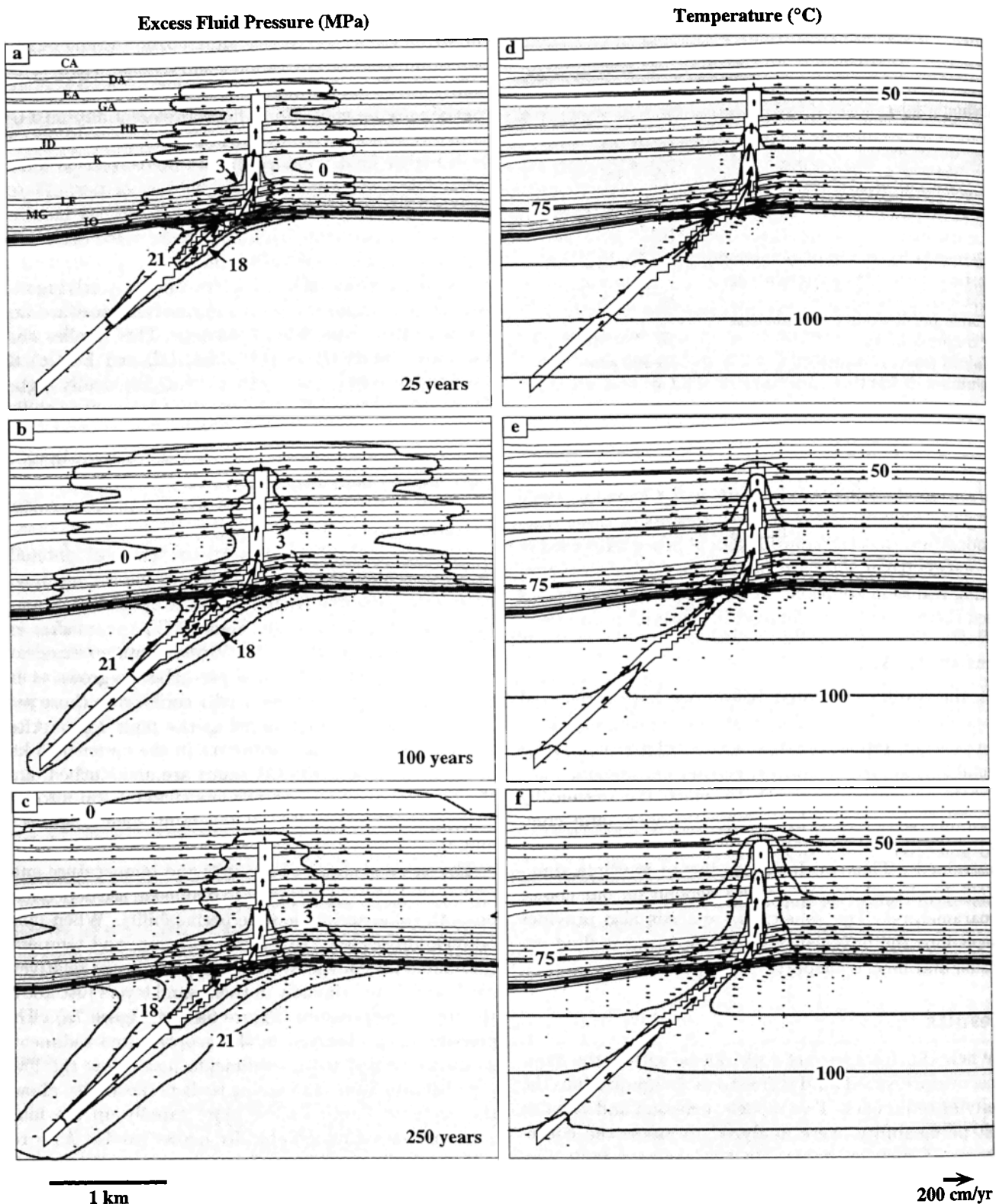


Figure 4. Excess fluid pressure and temperature predicted from the constant fault permeability simulations ($k_f = 10^{-14} \text{ m}^2$, $k_{h,\text{shale}} = 10^{-16} \text{ m}^2$, $k_{v,\text{shale}} = 10^{-17} \text{ m}^2$) at 25, 100, and 250 years after expulsion begins. Velocity vectors in the fault zone are scaled down by a factor of 5. No vertical exaggeration.

sured sediments when shale permeability decreases by 2 orders of magnitude, and flow in the geopressed section is essentially restricted to the fault zone and the permeable sand layer beneath the top of geopressure.

Lower permeability also restricts the ability of shales in the hydropressed zone to absorb expelled fluid. Preferential fluid flow along sand layers is also more pronounced when shale permeability drops (Figure 6c).

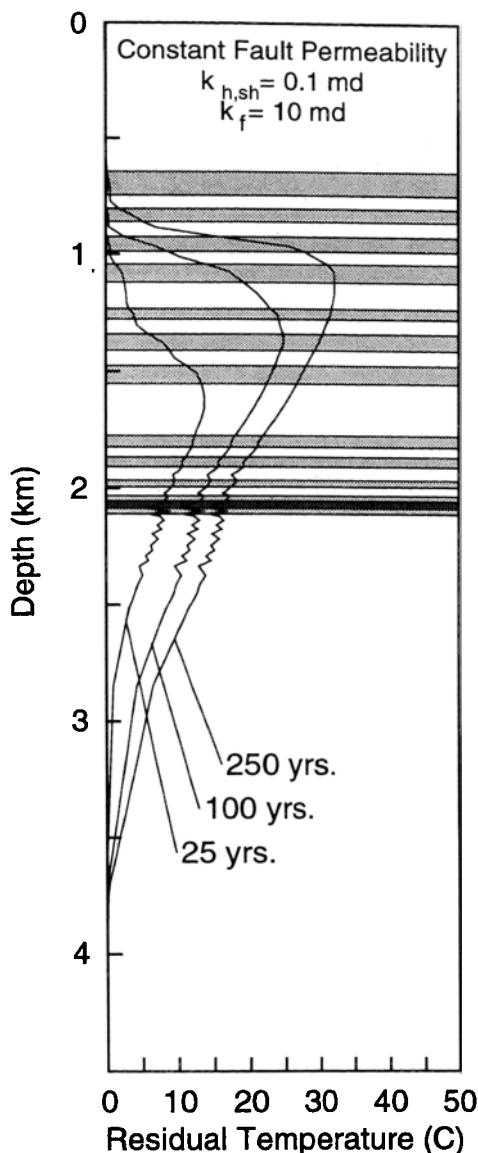


Figure 5. Residual temperature (model temperature minus initial temperature) predicted along the fault zone (section A-A' in Figure 3) for the constant fault permeability simulations shown in Figure 4.

Fluid flow along the fault (Figures 4b, 6b, and 6c) and the size and shape of thermal anomalies (Figure 7b) in the first several hundred years of an expulsion event are largely independent of shale permeability.

The depth to which the fault is hydraulically open within the geopressed zone also influences the size of temperature and pressure anomalies that form in the overlying sediments as fluid is expelled. As the penetration of the fault zone into the geopressed section decreases from 1.5 km to 0.5 km, the excess pressure anomaly at 100 years drops from over 3.5 MPa to less than 1.0 MPa (Figure 6d). The thermal anomaly also shrinks, from 24°C to 15°C at 100 years (Figure 7c).

Increasing the permeability of the low-permeability layer at the top of the geopressed section from 10^{-24} m² to 10^{-21} m² had no effect on the temperature and fluid pressure anomalies that formed over the duration

of our simulations. Further increasing the permeability of this layer to 10^{-18} m² allowed some fluid to leak vertically from the geopressed section into the overlying sediments, but the fluid pressure anomaly caused by this leakage was not apparent for several thousand years and even then was negligible.

After 10,000 years of continuous expulsion along the fault zone, excess fluid pressures in the geopressed zone predicted from the base model have decreased dramatically throughout much of the South Eugene Island minibasin, while excess pressures in the overlying sediments are as high as 6 MPa in sediments several kilometers from the fault zone (Figure 8a). These pressures are inconsistent with the elevated fluid pressures observed today in the Gulf of Mexico [e.g., Wallace *et al.*, 1979]. The thermal anomaly, which extends for several kilometers around the fault zone and is greater than 50°C (Figure 8b), is also much larger than any thermal anomalies reported in the region. The size of the temperature and pressure anomalies that form in the overlying sediments decreases as shale permeability decreases. In fact, when shale permeability is dropped by 2 orders of magnitude, drawdown of fluid pressure in the geopressed sediments is restricted to those sediments within 1 km of the fault zone and the permeable sand unit within the geopressed zone (Figure 8c). The corresponding thermal anomaly at 10,000 years is also much smaller (Figure 8d), but still significantly larger than the thermal anomaly observed in the study area.

Variable Fault Permeability Simulations

In the variable fault permeability simulations, fault permeability is dynamically computed as a function of fluid pressure, the number and width of fractures, and the compressibility of fault zone materials using equations (10) and (11). Results of these simulations indicate that fault zone permeability drops rapidly after an expulsion event is initiated (Figure 9). The drop in fault zone permeability is particularly pronounced during the first 1-10 years of an expulsion event, when rapid withdrawal of fluid along the fault zone causes fluid pressure in the geopressed sections of the fault zone to drop rapidly. As the expulsion event evolves, the fluid pressure in the fault zone just beneath the low-permeability layer reaches a quasi-steady state value, and fault zone permeability remains low but relatively constant. In spite of the low permeabilities calculated in the fault zone, fluid pressure has not dropped to the level required to close the fracture network even 1000 years after expulsion begins, and overpressured fluid continues to leak into the overlying sediments.

Temperature and excess pressure anomalies predicted using the variable fault permeability model (Figure 10) are smaller than those predicted from the constant fault permeability model (Figure 4). The pressure anomaly predicted from the variable fault permeability model grows laterally as fluid moves farther from the fault through the relatively permeable sand horizons in the sediments 1 km above the top of geopressure (Fig-

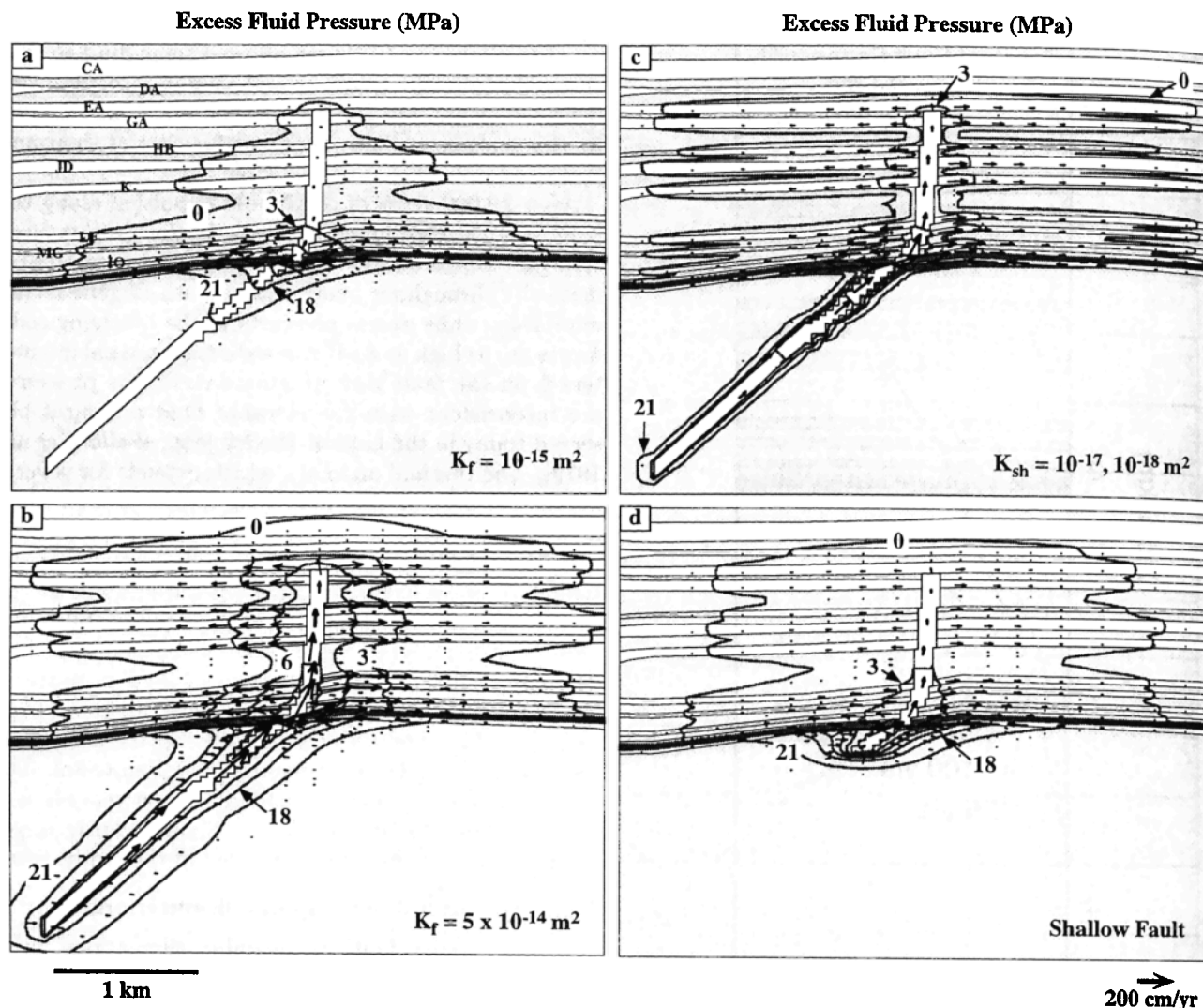


Figure 6. Excess fluid pressure predicted from the constant fault permeability simulations at 100 years after expulsion begins. Material properties are the same as for the simulations shown in Figure 4 unless otherwise noted: (a) $k_f = 10^{-15} \text{ m}^2$, (b) $k_f = 5 \times 10^{-14} \text{ m}^2$, (c) $k_{h,shale} = 10^{-17} \text{ m}^2$, $k_{v,shale} = 10^{-18} \text{ m}^2$, and (d) shallow fault. No vertical exaggeration.

ure 10a-10c). Little fluid enters higher sand layers (HB, JD, and K) intersected by the fault, and essentially no fluid flow is predicted in the sand layers above the fault (CA, DA, EA, and GA). Fluid is preferentially drawn from the abnormally pressured sediments south of the fault zone where the overpressured sand unit within the geopressed section is thicker. The thermal anomaly reaches a maximum value of approximately 7°C 100 years after expulsion begins and does not grow significantly as expulsion continues (Figures 10d-10f and Figure 11).

The size of temperature and pressure anomalies that form are dependent on the parameters used to calculate fault permeability. The compressibility of sediments in the fault zone is particularly important. When the value of this parameter is increased by an order of magnitude (from 10^{-12} to 10^{-11} Pa^{-1}), fault permeability drops to less than 10^{-15} m^2 in the first 2 years of the

event (Figure 9). As a result, the sizes of the temperature and pressure anomalies that form are dramatically reduced. After 100 years of expulsion, the pressure anomaly is restricted to those sand layers just above the low-permeability layer (Figure 12a), while the thermal anomaly has shrunk to less than 2.5°C (Figure 13a). Further reductions in fault zone compressibility cause fault permeability to drop to less than 10^{-16} m^2 almost immediately, and very little fluid is expelled.

Increasing the initial width of the fractures that form in the fault zone increases the size of the thermal and baric anomalies that form in the overlying sediments. When the initial fracture width is doubled, fault permeability drops at a much slower rate and remains relatively high as fluid continues to be expelled (Figure 9). Larger temperature and pressure anomalies form as a result of the increased fault zone permeability; after 100 years of expulsion, the pressure anomaly has moved

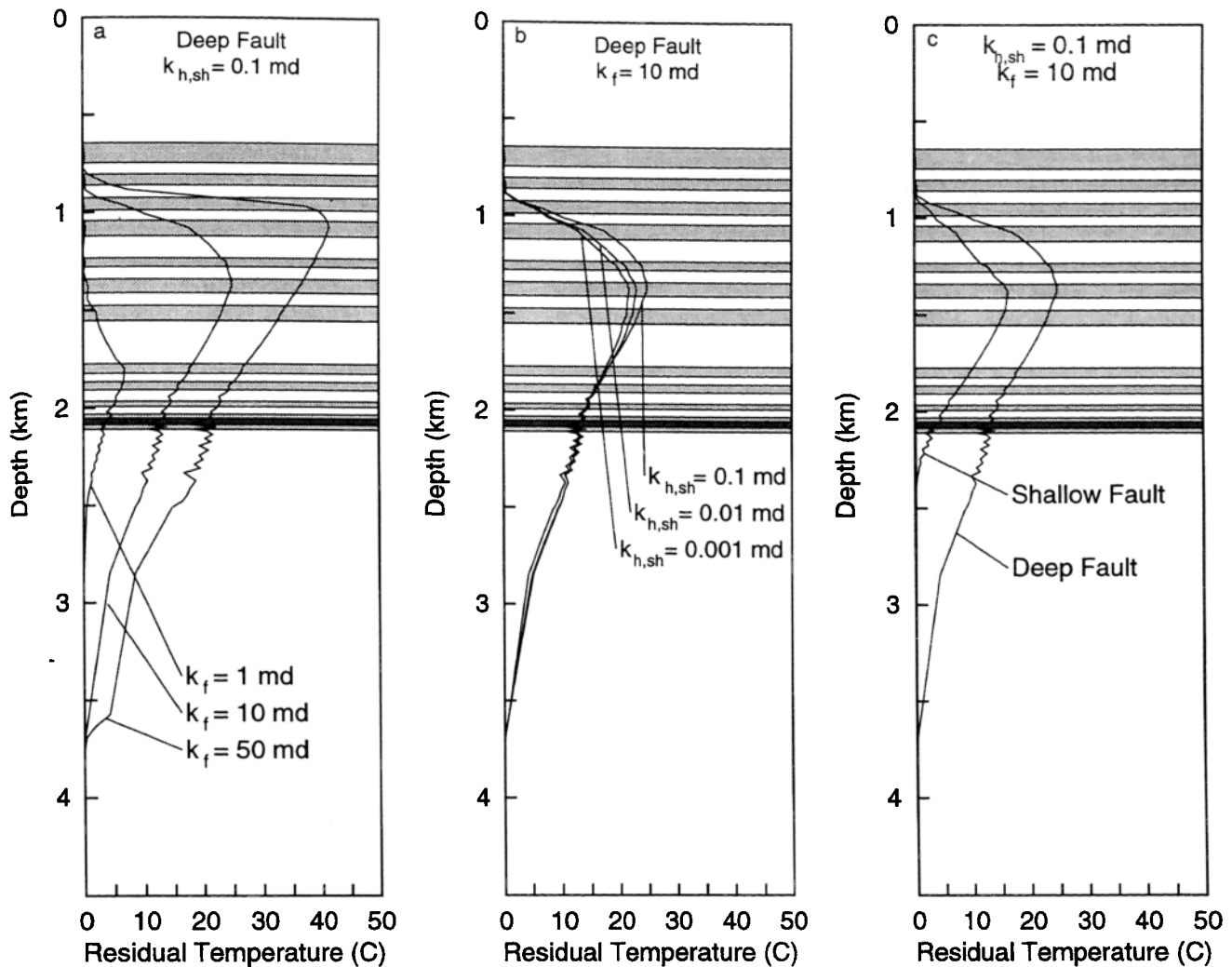


Figure 7. Residual temperature (model temperature minus initial temperature) at 100 years for the constant fault permeability simulations. Lightly shaded regions show the location of sand layers and the darker shading shows the location of the low-permeability layer at the top of geopressure.

into stratigraphically higher sediments (Figure 12b), while the thermal anomaly has grown to approximately 18°C (Figure 13b). Reducing the width of fractures reduces the size of temperature and pressure anomalies by a similar amount.

In contrast, increasing the number of fractures has a relatively small effect on the evolution of an expulsion event. Increasing the number of fractures from 1 to 2 to 5 increases fault zone permeability only in the first few years of an expulsion event (Figure 9). As a result, the pressure and temperature anomalies do not differ significantly (Figures 12c and 13c).

Fluid Flux

Results of the simulations indicate that large volumes of fluid are transferred from geopressed sediments into the overlying section in a geologically short period of time. The integrated fluid flux over the first 1000 years of expulsion, shown in Figure 14a for the constant fault

permeability models and in Figure 14b for the variable fault permeability models, is of the order of 100×10^6 kg fluid per horizontal square foot of the fault zone. Increasing the depth of the fault zone and the permeability of shales and sediments in the fault zone increases the amount of fluid expelled in the constant permeability models, while increasing the initial fracture width and decreasing the compressibility of materials in the fault zone increases the flux in the variable permeability models. In general, the amount of fluid expelled in the constant fault permeability model is 5 to 10 times larger than calculated from the variable fault permeability models.

Discussion

Results from both constant and variable fault permeability simulations indicate that pressure and temperature anomalies form a short time (<25 years) after the

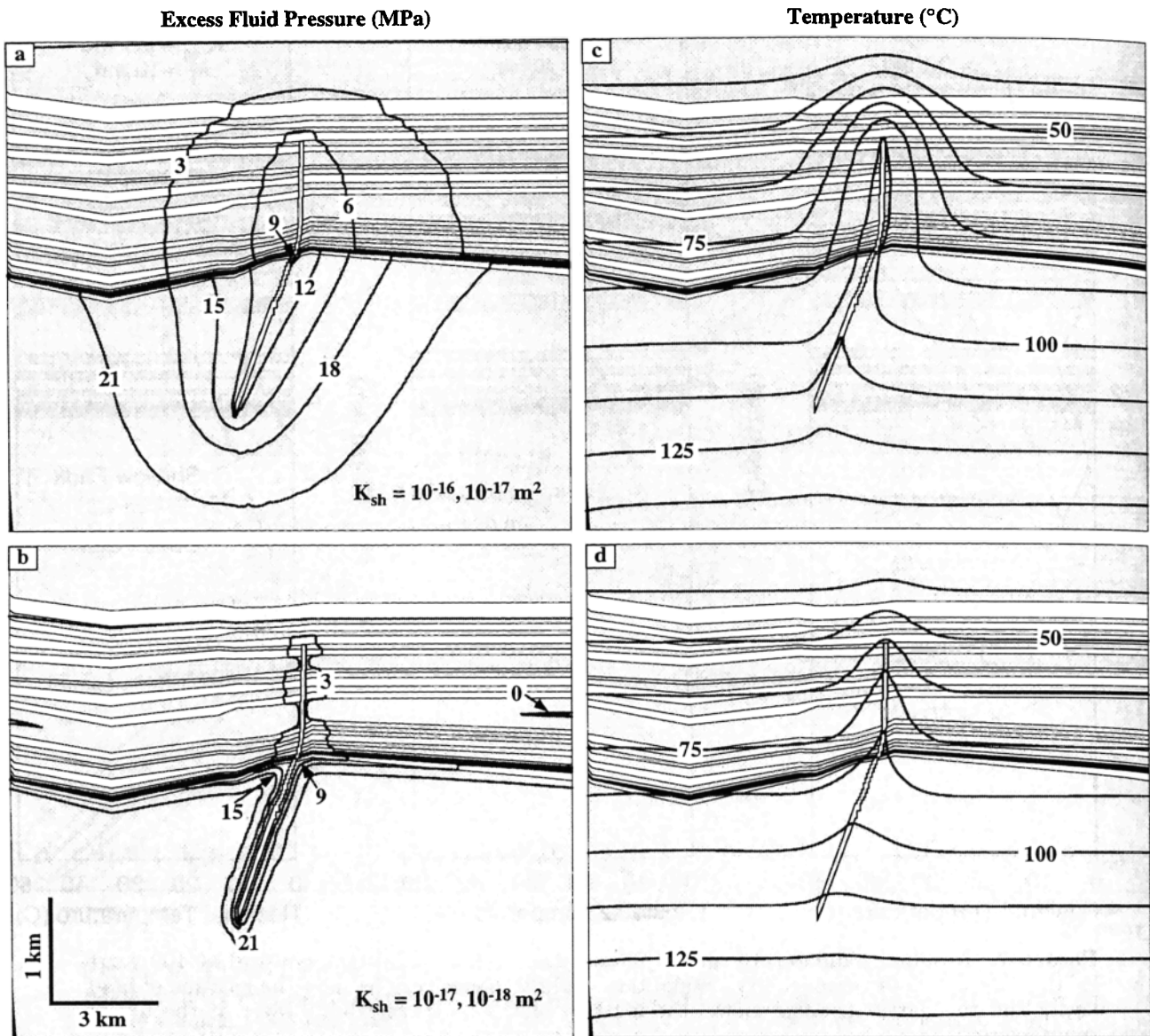
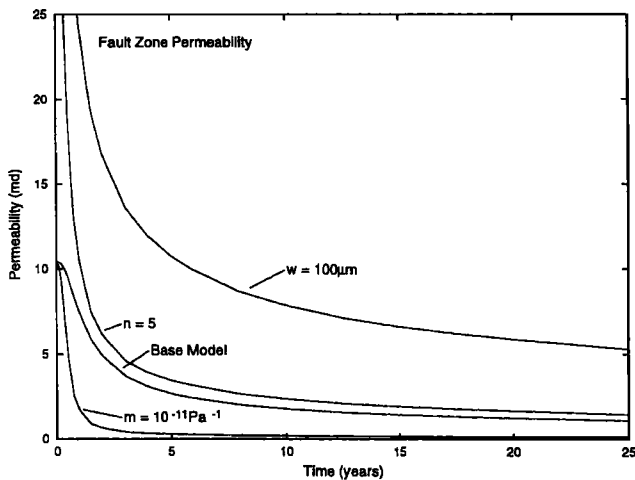


Figure 8. Excess fluid pressure and temperature predicted from the constant fault permeability simulations at 10,000 years after expulsion begins: (a) and (b) ($k_f = 10^{-14} \text{ m}^2$, $k_{h,\text{shale}} = 10^{-16} \text{ m}^2$, $k_{v,\text{shale}} = 10^{-17} \text{ m}^2$), (c) and (d) ($k_f = 10^{-14} \text{ m}^2$, $k_{h,\text{shale}} = 10^{-17} \text{ m}^2$, $k_{v,\text{shale}} = 10^{-18} \text{ m}^2$). Vertical exaggeration is 3:1.



fault zone becomes permeable and an expulsion event is initiated. These results are qualitatively consistent with data collected in the South Eugene Island area in that the pressure anomaly that forms is relatively broad and extends several kilometers into the sediments on either side of the fault while the thermal anomaly is much smaller and restricted to those sediments immediately to the south of the fault zone. Furthermore, the quantity of fluid expelled along the fault zone during the

Figure 9. Fault zone permeability computed as a function of time for the variable fault permeability simulations. Unless otherwise noted, $k_{h,\text{shale}} = 10^{-16} \text{ m}^2$, $k_{v,\text{shale}} = 10^{-17} \text{ m}^2$, $n = 1$, $w = 50 \mu\text{m}$, $m = 10^{-12} \text{ Pa}^{-1}$.

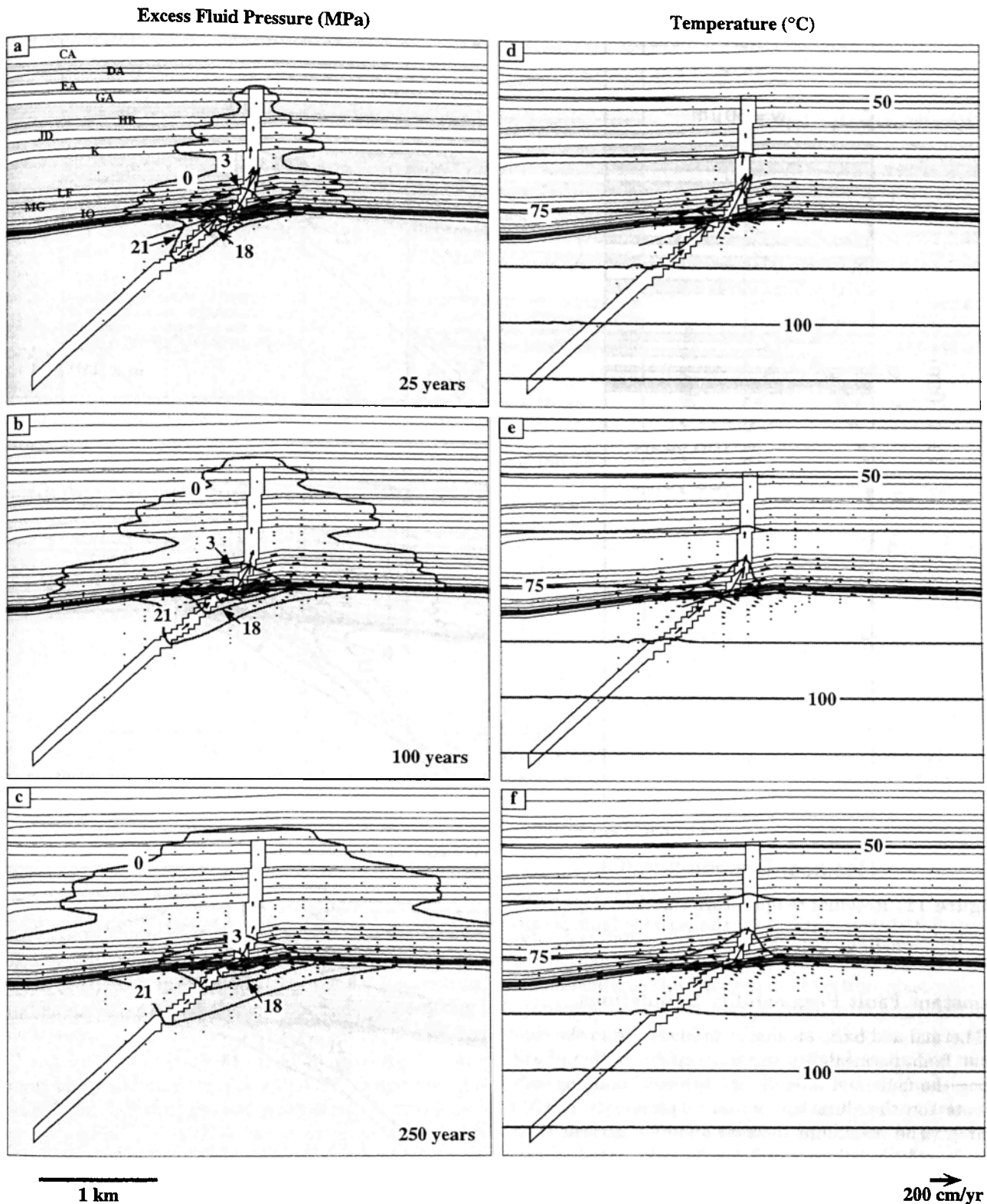


Figure 10. Excess fluid pressure and temperature predicted from the variable fault permeability simulations using the same parameters as in Figure 9 at 25, 100, and 250 years after expulsion begins. No vertical exaggeration.

first several hundred years of expulsion in the simulations is comparable to the amount of fluid removed from reservoirs in the South Eugene Island area since production began in 1972 [Anderson *et al.*, 1994]. The general

agreement between the the simulations and field data is consistent with the hypothesis that abnormally pressured fluids have recently been expelled along the Red Fault.

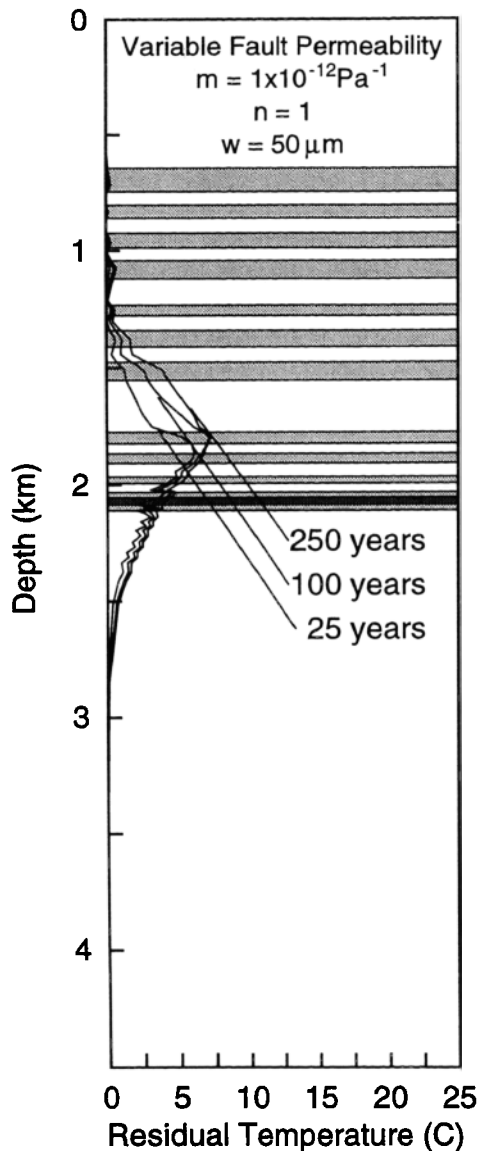


Figure 11. Residual temperature (model temperature minus initial temperature) for the variable fault permeability simulations.

Constant Fault Permeability Simulations

Thermal and baric anomalies predicted from the constant fault permeability expand rapidly both upward along the fault and laterally into the surrounding sediments for the duration of our experiments (10,000 years). The maximum thermal anomaly present soon after expulsion is initiated forms in sediments between 1.5 and 2 km depth; the maximum value then migrates upward to approximately 1 km depth within 250 years (Figure 5). Elevated fluid pressures are also predicted to form in the upper 1 km of sediments 100-250 years after the fault becomes permeable (Figure 4). Because there is no mechanism to close the fault in these simulations, the size of these anomalies continues to grow as fluid is expelled. In as little as 10,000 years after expulsion begins, a significant percentage of fluid has been removed from the overpressured section of the minibasin (Fig-

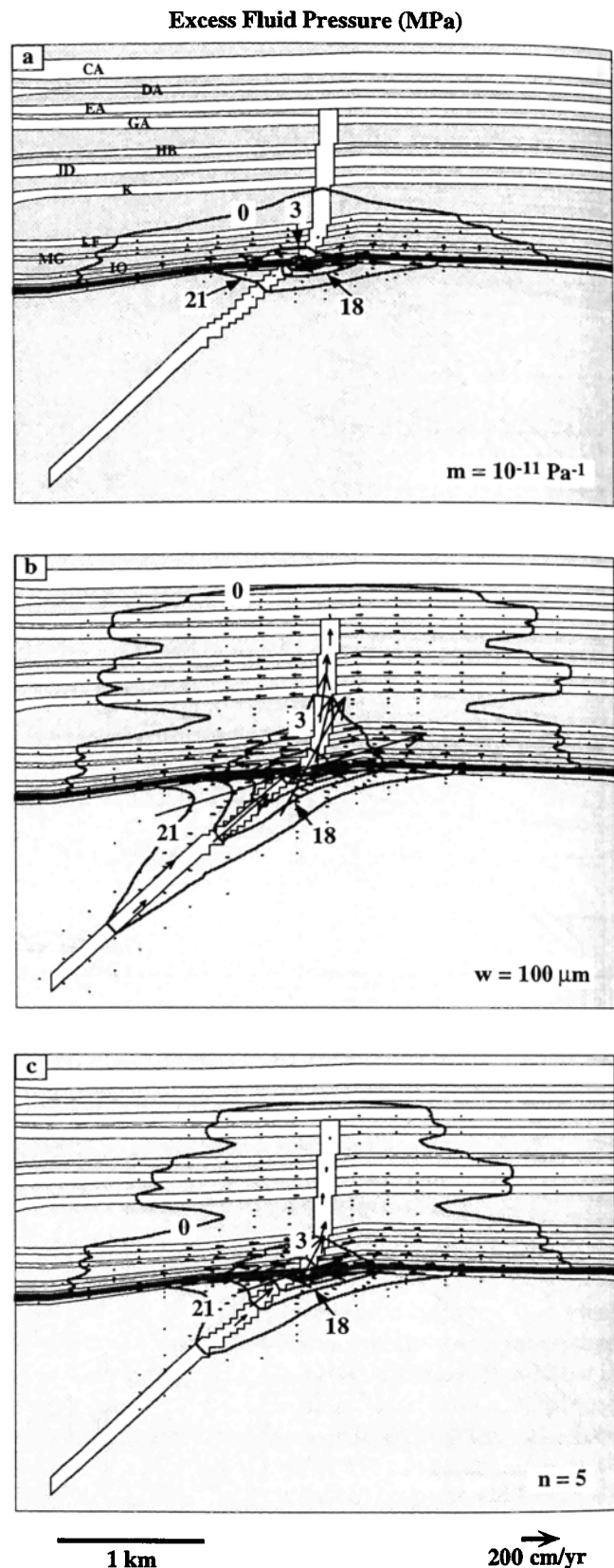


Figure 12. Excess fluid pressure predicted from the variable fault permeability simulations at 100 years after expulsion begins. Material properties are the same as for the simulations shown in Figure 9 unless otherwise noted: (a) $m = 10^{-11} \text{ Pa}^{-1}$, (b) $w = 100 \mu\text{m}$, (c) $n = 5$. No vertical exaggeration.

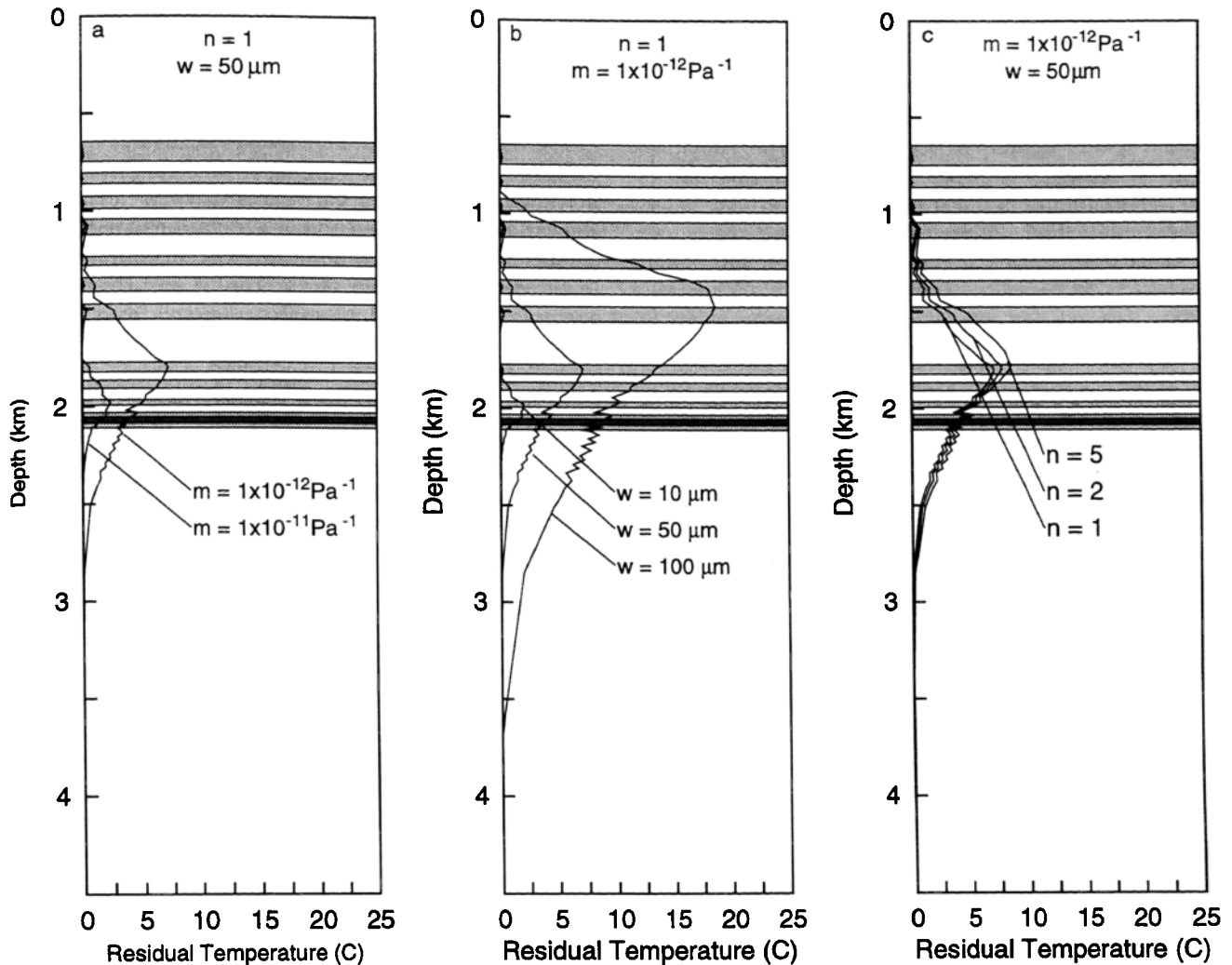


Figure 13. Residual temperature for the variable fault permeability simulations using the same material properties as listed in Figure 9 unless otherwise noted.

ure 8). Both thermal and baric anomalies predicted at this time are also much larger than those reported in the Gulf of Mexico, suggesting that fault zones penetrating into geopressed sediments do not remain permeable indefinitely.

A sensitivity analysis performed on the constant fault permeability simulations shows that the magnitude and shape of the resulting anomalies are sensitive to the permeability of the fault zone, the permeability of shales in the geopressed section, and the depth of the fault. In the simulations with high fault zone permeability, fluid migration is controlled by the permeable fault zone, which transmits significant amounts of fluid along its entire length into sediments far above the top of geopressure (Figure 6b). When a lower value of fault permeability is used, fluid movement occurs primarily along the permeable sands immediately above the top of geopressure, with little fluid flow observed in upper portions of the fault (Figure 6a). Thus, when fault permeability is low, the pressure anomaly moves laterally in

permeable horizons close to the low permeability layer rather than upward along the fault zone.

Sediments in the geopressed section must also be permeable enough to permit fluid to flow toward the fault zone for expulsion to occur (Figure 6c). Our results suggest that the geopressed sediments must have permeabilities of the order $5 \times 10^{-17} \text{ m}^2$ in order for sufficient fluid to be expelled to form temperature and pressure anomalies like those observed in the South Eugene Island area over timescales of 100 years. Although shales are generally thought to be relatively impermeable, shales near the top of geopressure in Eugene Island are significantly undercompacted, with porosities of 30% [Hart *et al.*, 1995]. According to the porosity-permeability function developed by Harrison and Summa [1991], this corresponds to a permeability of 10^{-17} m^2 . Moreover, Capuano [1993], suggests that open fracture networks may increase the permeability of geopressed shales to as high as 10^{-13} m^2 . Alternatively, relatively permeable sand layers that intersect

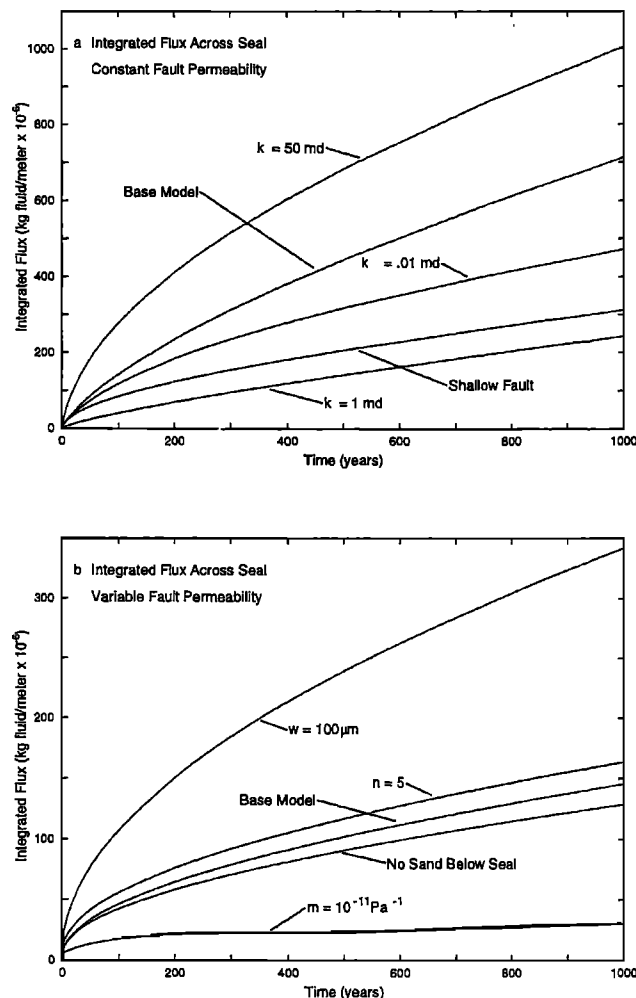


Figure 14. Integrated fluid flux across the top of geopressure for (a) constant fault permeability simulations and (b) variable fault permeability simulations. Material properties for the base model in Figure 14a are the same as those in Figure 4. Material properties for the base model in Figure 14b are the same as those in Figure 9.

the fault zone at depth may provide an alternate path for movement of overpressured fluid into the fault zone. Our results document the importance of permeable layers within the geopressed section; the drawdown of excess pressure in even a thin sand layer is sufficient to draw fluid from the surrounding shales and to increase the amount of fluid expelled.

A somewhat surprising result of the constant fault permeability simulations is that the thermal anomaly that developed during the first several hundred years of an expulsion event is independent of the shale permeability (Figure 7b). This suggests that most of the thermal energy transported along the fault originates from fluid residing within the deepest levels of the fault zone. The fact that the size of the thermal anomaly is reduced when the depth of the fault zone decreases (Figure 7c) is consistent with this conclusion. Therefore the existence of a large thermal anomaly related to

expulsion indicates that the fault along which the fluid is transported must be permeable at least 1 or 2 km into the geopressed sediments.

Variable Fault Permeability Simulations

In contrast to the constant fault permeability simulations, thermal and baric anomalies predicted from the variable fault permeability simulations are generally smaller (Figure 10) and reach their maximum values in the sediments closer to the top of geopressure. For example, the thermal anomaly predicted from the constant fault permeability model after 250 years of venting is almost 5 times higher than the 7°C anomaly predicted from the variable fault permeability model. The maximum thermal anomaly predicted from the variable fault permeability simulations at any given time is located in sediments deeper than 1.5 km depth, less than 0.5 km above the top of geopressure, and does not migrate upward with time (Figure 11).

A sensitivity analysis of the variable fault permeability simulations suggests that the quantity of fluid expelled and the size of thermal and baric anomalies that form are dependent on the amount of time the fault zone remains sufficiently permeable to permit expulsion. The permeability of the fault zone is, in turn, strongly dependent on the initial width of fractures that form in the fault zone and on the compressibility of surrounding sediments (Figure 9). Our results suggest that fractures must initially be wide enough to increase fault zone permeability to at least 10^{-14} m² and that the fault zone sediments must be incompressible enough to maintain permeabilities above 10^{-15} m² approximately 20-30 years after expulsion begins to transport sufficient fluid along the fault zone to form temperature and pressure anomalies similar to those observed in the South Eugene Island area.

Comparison of Constant and Variable Fault Permeability Simulations

Although the results are qualitatively similar, there are significant quantitative differences between the constant and variable fault permeability simulations. Thermal and baric anomalies predicted from the constant fault permeability simulations are generally larger than those from the variable fault permeability simulations. Furthermore, the thermal anomaly predicted from the constant fault permeability simulations reaches a maximum value in shallower sediments than that predicted from the variable fault permeability simulations. Finally, fault zone permeability predicted from the variable fault permeability simulations has dropped to relatively low values 100-200 years after expulsion begins, essentially shutting down the conduit and halting the growth of thermal and baric anomalies. However, the anomalies predicted from the constant fault permeability simulations continue to grow for several thousand years.

Fluid migration pathways predicted from the two models are also dramatically different. In both types of

simulations, fluid pressure rises first in the lower sands (Figures 4 and 10), suggesting they fill with expelled fluid sooner than the stratigraphically higher sands. In the variable fault permeability simulations, fault permeability decreases rapidly in the first years of an expulsion event (Figure 9), and the primary migration pathway for fluid is along the permeable sand layers (Figure 10) instead of vertically up the fault zone, as in the constant fault permeability simulations (Figure 4). The difference in migration pathways predicted from the constant and variable fault permeability models has important implications for petroleum exploration. If fault permeability remains high for several hundred years, hydrocarbons will eventually accumulate in the stratigraphically higher sands. However, if fault permeability is low or decreases with time as predicted from the variable fault permeability models, hydrocarbons will preferentially accumulate in the deeper sands just above the top of geopressure.

Comparison of Simulations With South Eugene Island Data

A quantitative comparison of the results obtained from our simulations with temperature and pressure data collected in the South Eugene Island area is necessary to determine whether the constant or variable fault permeability simulations more closely approximate observations. However, we do not expect results from either set of simulations to replicate data obtained from the South Eugene Island area because of the simplifications necessary to run our simulations. For example, the thermal field shown in Figure 2b results from both the salt domes on either side of the basin and expulsion of fluid along the fault zone. Because we were interested only in anomalies that formed from expulsion, we did not include the thermal effects of high thermal conductivity salt in our models, and thus the thermal fields predicted from our simulations are much simpler. Furthermore, both thermal and baric anomalies observed in the field have undoubtedly been influenced by the production of hydrocarbons from wells in the area. Fluid withdrawal was not included in our models.

It was also necessary to simplify the stratigraphy and structure to run our simulations. For example, we did not include the splay faults that offset isobars in Figure 2a in our simulations and therefore do not expect to replicate the pressure field observed in the field. Furthermore, we assumed all sediments above the low-permeability layer in our simulations were hydrostatically pressured while sediments beneath this layer were uniformly overpressured by 22 MPa. While the contours in Figure 2a suggest that there is a gradient in overpressures observed in the study area with higher values of overpressure deeper in the basin and some overpressuring of shallower sediments, there are also very few field data constraining fluid pressures in the geopressed section.

For the reasons described above, we do not expect our results to exactly replicate the temperature and pressure data collected in the field. Instead, we compare general features of the field data, such as the overall size and shape of the anomalies, the magnitude of anomalies, and the depth at which the maximum anomalies occur, to the results obtained from our simulations. This comparison suggests that variable fault permeability simulations more closely match observations than the constant fault permeability simulations. For example, the width of the thermal anomaly shown in Figure 2b is less than 2-3 km over the fault zone and reaches a maximum value at depths between 2.5 and 2.8 km. The thermal anomaly predicted from constant fault permeability simulations after only 100 years of expulsion is clearly larger than the 10-15°C anomaly associated with expulsion after the thermal effects of salt have been removed (G. Guerin, unpublished data, 1996) and reaches a maximum value in shallower sediments. Although the thermal anomaly obtained from the variable fault permeability is slightly smaller, reaching a maximum of 10°C, the fact that it reaches its maximum value in deeper sediments is clearly a better match to the field data.

The pressure anomaly predicted from the variable fault permeability simulations also matches the observed pressure field better than that obtained from the constant fault permeability simulations. The excess fluid pressure anomaly shown in Figure 2a does not extend into the upper 1500 m of sediments. Similarly, the excess fluid pressure anomaly predicted from the variable fault permeability simulations is essentially confined to sediments deeper than 1500 m below the surface (Figure 10). However, the excess fluid pressure anomaly obtained from the constant fault permeability simulations reaches the upper 0.5 km of sediment 100-250 years after expulsion begins (Figure 4).

Pressure anomalies predicted from both constant and variable fault permeability simulations differ from the field data in that predicted fluid pressures in the sediments beneath the top of geopressure decrease as fluid is expelled. No evidence for this decline is seen in Figure 2a. However, oil companies rarely drill into highly overpressured sediments, which is where we predict that fluid pressure is dropping. Moreover, fluid pressure drawdown should dissipate rapidly after expulsion stops. Therefore the absence of an observed pressure anomaly in highly overpressured sediments may simply reflect that there were insufficient pressure data at these depths. The thermal anomaly also differs in that it is located slightly to the south of the fault zone (Figure 2b) while our simulations predict that it should be centered over the fault zone.

Although one may argue that the quality of observational data collected in the South Eugene Island area is not sufficient to differentiate between the constant and variable fault permeability models, an analysis of the results presented above makes it clear that the expul-

sion of abnormally pressured fluid along faults like the Red Fault in the South Eugene Island area cannot last for geologically long time periods. When geopressured sediments are sufficiently permeable to permit expulsion and the fault zone remains permeable indefinitely, predicted fluid pressures in the geopressured zone drop significantly throughout the mini-basin after only 10,000 years of expulsion. These low fluid pressures are inconsistent with the elevated pore pressures observed throughout the Gulf of Mexico basin. Long periods of fluid expulsion also produce large thermal anomalies, which are not observed either. Furthermore, fluid pressure in the geopressured section of the fault zone drops by more than 10 MPa in the first 100 years of an expulsion event. This drop in fluid pressure should be sufficient to compact the incompletely consolidated shales that compose the fault zone, closing any open fractures and reducing fault zone permeability. Therefore the variable fault permeability simulations should more closely approximate fluid flow processes in the South Eugene Island area.

Limitations

The present study is a first attempt to incorporate a realistic hydrostratigraphy into simulations of fluid expulsion along faults that includes dynamic feedback between pore fluid pressure and fault permeability. Our results are qualitatively similar to observations in Eugene Island. In addition, this study places constraints on the duration of fluid expulsion and provides insights into the timing and pathways of secondary fluid migration from the top of the geopressured zone into overlying Plio-Pleistocene sand reservoirs.

A quantitative comparison of model results to observations in Eugene Island would require us to evaluate the potential effects of (1) pore fluid pressure dependent permeability in all stratigraphic layers; (2) fault zone permeability that varies spatially; (3) fluid withdrawal by pumping; and (4) a thicker pore pressure transition zone. These enhancements to our numerical model are the subject of current work. In addition, we are attempting to get better information on the permeability and compressibility of fault zone sediments from draw-down tests and laboratory experiments on core samples. Finally, because of the sensitivity of model results to the ability of surrounding sediments to provide and/or remove fluid from the fault zone, we plan to conduct 3-D simulations.

A more problematic extension of this study is to incorporate short-term secondary migration of fluids into the larger system of minibasin formation, generation of geopressure, and primary fluid migration. We know from geochemical studies that both the brines and hydrocarbons in Plio-Pleistocene reservoirs in Eugene Island are coming from Paleogene or older source rocks 5-12 km below the seafloor [Whelan *et al.*, 1994a,b]. Currently, there are neither well or seismic reflection data available for these deeply buried sediments. Thus

any attempt to simulate pore pressure generation, fluid flow, and heat transport on a regional scale over geologic time must be speculative and underconstrained.

Conclusions

Results obtained from this study show that temperature and pressure anomalies that form as abnormally pressured fluid is expelled along a permeable fault zone are generally consistent with those observed in the South Eugene Island area, offshore Louisiana. Furthermore, results obtained from the variable fault permeability simulations, in which fault permeability decreases as fluid pressure drops, match data collected in the South Eugene Island area better than those simulations in which fault permeability remains constant. This observation and model results suggesting that temperature and pressure anomalies generated by long-term fluid expulsion are inconsistent with observations in the Gulf of Mexico demonstrate that expulsion of abnormally pressured fluid along fault zones is not continuous.

A sensitivity analysis reveals that sediments in the geopressured section must be relatively permeable for significant expulsion to occur. Sediments may be permeable because of undercompaction or fractures in the overpressured shales or because interbedded sand layers are present. We have also shown that high fault zone permeabilities transport fluid from the abnormally pressured sediments to stratigraphically higher levels, while fluid movement occurs primarily through lower sands immediately above the top of geopressure when fault zone permeability is low. Changes in fault zone permeability in the variable permeability models are strongly dependent on the properties of the fault zone, in particular, the initial width of fractures that form and the compressibility of adjacent sediments. Fault zone permeability in these simulations must remain above approximately 10^{-15} m^2 for 20-30 years after expulsion begins to generate temperature and pressure anomalies similar to those observed in the South Eugene Island area.

Acknowledgments. We thank Paul Manhardt for assistance in adapting the Akcess.Basin software for this study; Dimas Coehlo, Laurel Alexander, Peter Flemings, and Roger Anderson for informative discussions regarding the South Eugene Island area; and Gilles Guerin for providing us with the thermal field in the South Eugene Island area prior to publication. Vishnu Ranganathan, Mark Person and Robert Lowell are thanked for their detailed reviews, which substantially improved the content of this manuscript. This work was supported by the U.S. Department of Energy (DE-FC22-93BC14961) and the Global Basins Research Network.

References

- Aharon, P., H. H. Roberts, and R. Snelling, Submarine venting of brines in the deep Gulf of Mexico: Observations and geochemistry, *Geology*, 20, 483-486, 1992.

- Alexander, L. L., and P. B. Flemings, Geologic evolution of a Pliocene-Pleistocene salt withdrawal mini-basin: Eugene Island Block 330, offshore Louisiana, *AAPG Bull.*, *79*, 1737-1756, 1995.
- Anderson, R. N., Recovering dynamic Gulf of Mexico reserves and the U.S. energy future, *Oil Gas J.*, *11*, 85-91, 1993.
- Anderson, R. N., W. He, M. A. Hobart, C. R. Wilkinson, and H. R. Nelson, Active fluid flow in the Eugene Island area, offshore Louisiana, *Geophys. Leading Edge Explor.*, *89*, 12-17, 1991.
- Anderson, R. N., P. Flemings, S. Losh, J. Austin, and R. Woodhams, Gulf of Mexico growth fault drilled, seen as oil, gas migration pathway, *Oil Gas J.*, *12*, 97-102, 1994.
- Antonellini, M. and A. Aydin, Effect of faulting on fluid flow in porous sandstones: Petrophysical properties, *AAPG Bull.*, *78*, 355-377, 1994.
- Baker, A. J., and D. W. Pepper, *Finite Elements 1-2-3*, 341 pp., McGraw-Hill, New York, 1991.
- Barker, C., Aquathermal pressuring-role of temperature in development of abnormal-pressure zones, *AAPG Bull.*, *56*, 2068-2071, 1972.
- Bekins, B. A., A. M. McCaffrey, and S. J. Dreiss, Episodic and constant flow models for the origin of low-chloride waters in a modern accretionary complex, *Water Resour. Res.*, *31*, 3205-3215, 1995.
- Bennett, S. S., and J. S. Hanor, Dynamics of subsurface salt dissolution at the Welsh Dome, Louisiana Gulf Coast, *Dynamical Geology of Salt and Related Structures*, edited by I. Lerche and J. J. O'Brien, pp. 653-677, Academic, San Diego, Calif., 1987.
- Bethke, C. M., A numerical model of compaction-driven groundwater flow and heat transfer and its applications to the paleohydrology of intracratonic sedimentary basins, *J. Geophys. Res.*, *90*, 6817-6828, 1985.
- Bethke, C. M., Inverse hydrologic analysis of the distribution and origin of Gulf Coast-type geopressured zones, *J. Geophys. Res.*, *91*, 6535-6545, 1986.
- Brantley, S. L., B. Evans, S. H. Hickman, and D. A. Crear, Healing of microcracks in quartz: Implications for fluid flow, *Geology*, *18*, 136-139, 1990.
- Bredehoeft, J. D. and B. B. Hanshaw, On the maintenance of anomalous fluid pressures, I, Thick sedimentary sequences, *Geol. Soc. Am. Bull.*, *79*, 1097-1106, 1968.
- Bredehoeft, J. D., J. B. Wesley, and T. D. Fouch, Simulations of the origin of fluid pressure, fracture generation, and the movement of fluids in the Uinta Basin, Utah, *AAPG Bull.*, *78*, 1729-1747, 1994.
- Brown, K. M., The variation of the hydraulic conductivity structure of an overpressured thrust zone with effective stress, *Proc. Ocean Drill. Program, Sci. Results*, *146*, 281-289, 1995.
- Bruce, C. H., Smectite dehydration—Its relation to structural development and hydrocarbon accumulation in northern Gulf of Mexico basin, *AAPG Bull.*, *68*, 673-683, 1984.
- Bruton, D. J., and H. C. Helgeson, Calculation of the chemical and thermodynamic consequences of differences between fluid and geostatic pressure in hydrothermal systems, *Am. J. Sci.*, *283-A*, 540-588, 1983.
- Capuano, R. M., Hydrochemical constraints on fluid-mineral equilibria during compaction diagenesis of kerogen-rich geopressured sediments, *Geochim. Cosmochim. Acta*, *54*, 1283-1299, 1990.
- Capuano, R. M., Evidence of fluid flow in microfractures in geopressured shales, *AAPG Bull.*, *77*, 1303-1314, 1993.
- Carson, B., E. Suess, and J. C. Strasser, Fluid flow and mass flux determinations at vent sites on the Cascadia margin accretionary prism, *J. Geophys. Res.*, *95*, 8891-8898, 1990.
- Cathles, L. M., and A. T. Smith, Thermal constraints on the formation of Mississippi Valley-type lead-zinc deposits and their implications for episodic basin dewatering and deposit genesis, *Econ. Geol.*, *78*, 983-1002, 1983.
- Cipriani, F. D., L. M. Cathles, and P. D. Manhardt, Simulating salt diapirism, overpressuring, and seal rupture in sedimentary basins (abstract), *Eos Trans. AGU*, *74*(16), Spring Meet. Suppl., 155, 1993.
- Coehlo, D., L. Alexander, F. Cipriani, L. Cathles, S. Roberts, and J. Nunn, Modeling fluid flow along listric growth faults in the Eugene Island Block 330 Field, Gulf of Mexico, paper presented at 1994 AAPG Annual Convention, *Am. Assoc. of Pet. Geol.*, Denver, Colorado, 1994.
- Davis, E. E., R. D. Hyndman, and H. Villinger, Rates of fluid expulsion across the northern Cascadia accretionary prism: Constraints from new heat flow and multichannel seismic reflection data, *J. Geophys. Res.*, *95*, 8869-8889, 1990.
- Deming, D., Factors necessary to define a pressure seal, *AAPG Bull.*, *78*, 1005-1009, 1994.
- Dickinson, G., Geological aspects of abnormal reservoir pressures in Gulf Coast Louisiana, *AAPG Bull.*, *37*, 410-432, 1953.
- Downey, M. W., Evaluating seals for hydrocarbon accumulations, *AAPG Bull.*, *68*, 1752-1763, 1984.
- Engelder, T., *Stress Regimes in the Lithosphere*, 457 pp., Princeton Univ. Press, Princeton, N. J., 1993.
- Fisher, A. T., and M. W. Hounslow, Transient fluid flow through the toe of the Barbados accretionary complex: Constraints from Ocean Drilling Program Leg 110 heat flow studies and simple models, *J. Geophys. Res.*, *95*, 8845-8858, 1990.
- Flemings, P. B., L. L. Alexander, and R. N. Anderson, The hydrostratigraphy of a Plio-Pleistocene growth fault: The Eugene Island Block 330 Field, in *Department of Energy Quarterly Technical Report* edited by R. N. Anderson, Washington, D.C., 1994.
- Foucher, J. P., X. L. Pichon, S. Lallemand, M. A. Hobart, P. Henry, M. Benedetti, G. K. Westbrook, and M. G. Langseth, Heat flow, tectonics, and fluid circulation at the toe of the Barbados ridge accretionary prism, *J. Geophys. Res.*, *95*, 8859-8867, 1990.
- Fowler, W. A., Pressures, hydrocarbon accumulation, and salinities—Chocolate Bayou Field, Brazoria County, Texas, *J. Petrol. Technol.*, *22*, 411-423, 1970.
- Freed, R. L., and D. R. Peacor, Geopressured shale and sealing effect of smectite to illite transition, *AAPG Bull.*, *73*, 1223-1232, 1989.
- Garven, G., S. Ge, M. A. Person, and D. A. Sverjensky, Genesis of stratabound ore deposits in the midcontinent basins of North America, 1, The role of regional groundwater flow, *Am. J. Sci.*, *293*, 497-568, 1993.
- Haneberg, W. C., Steady state groundwater flow across idealized faults, *Water Resour. Res.*, *31*, 1815-1820, 1995.
- Harrison, W. J., and L. L. Summa, Paleohydrology of the Gulf of Mexico Basin, *Am. J. Sci.*, *291*, 109-176, 1991.
- Hart, B. S., P. B. Flemings, and A. Deshapande, Porosity and pressure: Role of compaction disequilibrium in the development of geopressures in a Gulf Coast Pleistocene basin, *Geology*, *23*, 45-48, 1995.
- Hedberg, H. H., Relation of methane generation to undercompacted shales, shale diapirs, and mud volcanoes, *AAPG Bull.*, *58*, 661-673, 1974.
- Henry, P., X. L. Pichon, S. Lallemand, J.-P. Foucher, G. Westbrook, and M. Hobart, Mud volcano field seaward of the Barbados accretionary complex: A deep-towed side scan sonar survey, *J. Geophys. Res.*, *95*, 8917-8928, 1990.
- Hickman, S. H., and B. Evans, Diffusional crack healing in calcite: The influence of crack geometry upon healing rate, *Phys. Chem. Miner.*, *15*, 91-102, 1987.

- Holland, D. S., J. J. Leedy, and D. R. Lammlein, Eugene Island Block 330 field-U.S.A offshore Louisiana, in *Structural Traps III: Tectonic Fold and Fault Traps, Treatise Pet. Geol.*, edited by E. A. Beaumont and N. H. Foster, pp. 103-143, 1990.
- Hooper, E. C. D., Fluid migration along growth faults in compacting sediments, *J. Pet. Geol.*, *14*, 161-180, 1991.
- Hunt, I. M., Generation and migration of petroleum from abnormally pressured fluid compartments, *AAPG Bull.*, *74*, 1-12, 1990.
- Jouniaux, L., S. Lallemand, and J.-P. Pozzi, Changes in the permeability, streaming potential and resistivity of a claystone from the Nankai prism under stress, *Geophys. Res. Lett.*, *21*, 149-152, 1994.
- Knipe, R. J., The influence of fault zone processes and diagenesis on fluid flow, in *Diagenesis and Basin Development*, edited by A. D. Horbury and A. G. Robinson, *AAPG Stud. Geol.*, *36*, 135-151, 1993.
- Lewis, B. T. R., and G. C. Cochrane, Relationship between the location of chemosynthetic benthic communities and geologic structure on the Cascadia subduction zone, *J. Geophys. Res.*, *95*, 8783-8793, 1990.
- Lopez, D. L., and L. Smith, Fluid flow in fault zones: analysis of the interplay of convective circulation and topographically driven groundwater flow, *Water Resour. Res.*, *31*, 1489-1503, 1995.
- Losh, S. and J. Wood, Brine chemistry, Blocks 330 and 316, in *Results of the Pathfinder Drilling Program into a Major Growth Fault: Part of the GBRN/DOE Dynamic Enhanced Recovery Project in Eugene Island 330 Field, Gulf of Mexico* edited by R. N. Anderson et al., pp. 250-261, LDEO Press, Palisades, N. Y. 1994.
- Lowell, R. P., Thermoelasticity and the formation of black smokers, *Geophys. Res. Lett.*, *17*, 709-712, 1990.
- Moore, G. F., T. H. Shipley, P. L. Stoffa, D. E. Karig, A. Taira, S. Kuramoto, H. Tokuyama, and K. Suyehiro, Structure of the Nankai Trough accretionary zone from multichannel seismic reflection data, *J. Geophys. Res.*, *95*, 8753-8765, 1990a.
- Moore, J. C., D. Orange, and L. D. Kulm, Interrelationship of fluid venting and structural evolution: Alvin observations from the frontal accretionary prism, Oregon, *J. Geophys. Res.*, *95*, 8795-8808, 1990b.
- Neuzil, C. E., Abnormal pressures as hydrodynamic phenomena, *Am. J. Sci.*, *295*, 742-786, 1995.
- Nunn, J. A., Free thermal convection beneath intracratonic basins: Thermal and subsidence effects, *Basin Res.*, *6*, 115-130, 1994.
- Ortoleva, P., Z. Al-Shaieb, and J. Puckette, Genesis and dynamics of basin compartments and seals, *Am. J. Sci.*, *295*, 345-427, 1995.
- Palciauskas, V. V., and P. A. Domenico, Microfracture development in compacting sediments: Relation to hydrocarbon-maturation kinetics, *AAPG Bull.*, *64*, 927-937, 1980.
- Palciauskas, V. V., and P. A. Domenico, Fluid pressures in deforming porous rocks, *Water Resour. Res.*, *25*, 203-213, 1989.
- Powers, M. C., Fluid release mechanisms in compacting marine mudrocks and their importance in oil exploration, *AAPG Bull.*, *51*, 1240-1254, 1967.
- Powley, D. E., Pressures and hydrogeology in petroleum basins, *Earth Sci. Rev.*, *29*, 215-226, 1990.
- Ranganathan V., Basin dewatering near salt domes and formation of brine plumes, *J. Geophys. Res.*, *97*, 4667-4683, 1992.
- Ranganathan, V., and J. S. Hanor, Perched brine plumes above salt domes and dewatering of geopressed sediments, *J. Hydrol.*, *110*, 63-86, 1989.
- Roberts, S. J., and J. A. Nunn, Episodic fluid expulsion from geopressed sediments, *Mar. Pet. Geol.*, *12*, 195-204, 1995.
- Screaton, E. J., D. R. Wuthrich, and S. J. Dreiss, Permeabilities, fluid pressures, and flow rates in the Barbados ridge complex, *J. Geophys. Res.*, *95*, 8997-9007, 1990.
- Sharp, J. M., Permeability controls on aquathermal pressuring, *AAPG Bull.*, *67*, 2057-2061, 1983.
- Shi, Y., C.-T. Wang, and W. Hwang, Hydrogeological modeling of porous flow in the Oregon accretionary prism, *Geology*, *17*, 321-323, 1989.
- Sibson, R. H., Conditions for fault-valve behavior, in *Deformation Mechanisms, Rheology and Tectonics*, edited by R. J. Knipe and E. H. Rutter, *Geol. Soc. London, Spec. Publ.* *54*, 15-28, 1990.
- Smith, D. A., Sealing and nonsealing faults in Louisiana gulf coast salt basin, *AAPG Bull.*, *64*, 145-172, 1980.
- Smith, L., and D. S. Chapman, On the thermal effects of groundwater flow, 1, Regional scale systems, *J. Geophys. Res.*, *88*, 899-913, 1983.
- Snow, D. T., Rock fracture spacings, openings, and porosities, *J. Soil Mech.*, *94*, 73-91, 1968.
- Spencer, C. W., Hydrocarbon generation as a mechanism for overpressuring in Rocky Mountain region, *AAPG Bull.*, *71*, 368-388, 1987.
- Wallace, R. H., T. F. Kraemer, R. E. Taylor, and J. B. Weselmann, Assessment of geopressed-geothermal resources in the northern Gulf of Mexico basin, *U. S. Geol. Surv. Circ.* *790*, 132-155, 1979.
- Weedman, S. D., S. L. Brantley, and W. Albrecht, Secondary compaction after secondary porosity: Can it form a pressure seal?, *Geology*, *20*, 303-306, 1992.
- Westbrook, G. K., and M. J. Smith, Decollements and mud volcanos: Evidence from the Barbados Ridge Complex for the role of high pore-fluid pressure in the development of an accretionary complex, *Geology*, *11*, 279-283, 1983.
- Whelan, J., L. Eglington, R. Requejo, and M. C. Kennicutt, Pathfinder well organic geochemical-indicators of oil source and maturity and fluid flow mechanisms, in *Results of the Pathfinder Drilling Program into a Major Growth Fault: Part of the GBRN/DOE Dynamic Enhanced Recovery Project in Eugene Island 330 Field, Gulf of Mexico* edited by R. N. Anderson et al., pp. 250-261, LDEO Press, Palisades, N. Y., 1994a.
- Whelan, J. K., M. C. Kennicutt II, J. M. Brooks, D. Schumacher, and L. B. Eglington, Organic geochemical indicators of dynamic fluid flow processes in petroleum basins, *Org. Geochem.*, *22*, 587-615, 1994b.
- Wieck, J., M. Person, and D. S. Chapman, A new finite element model for simulating fault block motion and hydrothermal fluid flow within rifting basins, *Water Resour. Res.*, *31*, 3241-3258, 1995.
- Williams, M. D., and V. Ranganathan, Ephemeral thermal and solute plumes formed by upwelling groundwaters near salt domes, *J. Geophys. Res.*, *99*, 15,667-15,681, 1994.
- Yassir, N. A., and J. S. Bell, Relationships between pore pressure, stresses, and present-day geodynamics in the Scotian Shelf, offshore eastern Canada, *AAPG Bull.*, *78*, 1863-1880, 1994.

L. Cathles and F.-D. Cipriani, Department of Geological Sciences, Cornell University, Ithaca, NY 14853. (e-mail: cathles@geology.tn.cornell.edu)

J. A. Nunn, Department of Geology and Geophysics, Louisiana State University, Baton Rouge, LA 70803. (e-mail: jeff@sqirt.geol.lsu.edu)

S. J. Roberts, Department of Geology, Bowling Green State University, Bowling Green, OH 43403. (e-mail: sjrober@bgnet.bgsu.edu)

(Received December 4, 1995; revised August 23, 1996; accepted August 27, 1996.)